MODELING AND REDUCTION OF SHAFT VOLTAGES IN AC MOTORS FED BY FREQUENCY CONVERTERS
Doctoral Dissertation

Petri Mäki-Ontto

Helsinki University of Technology
Department of Electrical and Communications Engineering
Power Electronics Laboratory

MODELING AND REDUCTION OF SHAFT VOLTAGES IN AC MOTORS FED BY FREQUENCY CONVERTERS
Doctoral Dissertation

Petri Mäki-Ontto

Dissertation for the degree of Doctor of Science in Technology to be presented with due permission of the Department of Electrical and Communications Engineering for public examination and debate in Auditorium S4 at Helsinki University of Technology (Espoo, Finland) on the 21st of April, 2006, at 12 noon.

Helsinki University of Technology
Department of Electrical and Communications Engineering
Power Electronics Laboratory

Teknillinen korkeakoulu
Sähkö- ja tietoliikennetekniikan osasto
Tehoelektroniikan laboratorio

Author   Petri Mäki-Ontto

Name of the dissertation

Modeling and reduction of shaft voltages in ac motors fed by frequency converters

Abstract

This thesis deals with the modeling and mitigation of shaft voltages and bearing currents in frequency converter-fed ac motors. Common-mode voltages produced by modern frequency converters can cause destructive currents in motor bearings. The distribution of the common-mode voltage between parasitic capacitances in the motor causes a capacitive shaft voltage, and high-frequency common-mode currents flowing in the stator core generate a shaft-encircling magnetic flux, which causes an induced shaft voltage. Simulation models for these phenomena are needed in the evaluation of new drive system designs that could cause shaft voltage problems. Methods for the mitigation of shaft voltages can also be investigated by such models. In the thesis, the circumferential magnetic flux that causes the induced shaft voltage is investigated experimentally and by numerical analysis. Analytical expressions are derived for the magnetic flux and the common-mode impedance of the stator core. A circuit model suitable for the shaft voltage analysis is developed for induction motors. Both the capacitive and induced shaft voltages are included in the model. A correct common-mode impedance distribution of the drive system in a wide frequency band is essential in the shaft voltage analysis. Therefore, the circuit models of all drive system components are developed, and a complete model of the electric drive is composed. The model is validated by comparing the simulations to experimental results. Some promising methods for bearing current mitigation in high-power low-voltage drives are investigated in the thesis using simulations, analytical expressions, and experiments. New design principles are proposed for mitigating the shaft voltages in induction motors.

Väitöskirjan nimi

Taajuusmuuttajalla syötetyissä vaihtovirtamoottoreissa syntyvän akselijännitteen mallintaminen ja vähentäminen

Tiivistelmä

Väitöskirja käsittelee taajuusmuuttajalla syötetyissä vaihtovirtamoottoreissa syntyvien akseli-jännitteiden ja laakerivirtojen mallintamista ja vähentämistä. Nykyaikaisten taajuusmuuttajien tuottama yhteismuotoinen jännite saattaa aiheuttaa tuhoisia virtoja sähkömoottorin laakereissa. Yhteismuotoisen jännitteen jakautuminen moottorin parasiittisissa kapasitansseissa aiheuttaa kapasitiivisen akselijännitteen, ja staattorilevysydämen läpi kulkevat suurtaajuiset yhteismuotoiset sähkövirrat synnyttävät akselin kiertävän magneettivuon, joka aiheuttaa indusoituneen akselijännitteen. Uuden sähkökäyttöjärjestelmän suunnittelussa tarvitaan simulointimalleja, joiden avulla voidaan tutkia, aiheuttaako järjestelmä mahdollisesti laakerivirtaongelmia. Tällaisilla malleilla voidaan myös tutkia akselijännitteiden pienennysmenetelmiä. Väitöskirjassa on tutkittu kokeellisesti ja numeerisilla menetelmillä moottorin akselia kiertävää suurtaajuista magneettivuota, joka aiheuttaa indusoituneen akselijännitteen. Magneettivuolle ja staattorilevysydämen yhteismuotoiselle impedanssille on johdettu analyyttiset yhtälöt. Epätahtimoottorille on kehitetty piirimalli, joka soveltuu akselijännitteiden analysointiin ja johon on sisällytetty sekä kapasitiivinen että indusoitunut akselijännite. Sähkökäytön yhteismuotoisen impedanssin jakautumisen tunteminen laajalla taajuusalueella on välttämätöntä akselijänniteanalyysissä. Siksi väitöskirjassa on kehitetty kaikkien sähkökäytön komponenttien piirimallit ja laadittu järjestelmän kokonaismalli. Mallin oikeellisuus on tarkistettu vertaamalla simulointituloksia mitattuihin tuloksiin. Lupaavia menetelmiä laakerivirtojen pienentämiseksi on tutkittu työssä simuloinneilla, analyyttisilla lausekkeilla ja kokeellisesti. Työssä on myös ehdotettu uusia laakerivirtojen pienentämiseen tähtääviä epätahtikoneiden suunnitteluperiaatteita.

Preface

This work was carried out at the Power Electronics Laboratory at Helsinki University of Technology. I express my gratitude to Prof. Jorma Luomi for his excellent supervision in this project. I would also like to thank Mr. Henri Kinnunen, who co-authored three papers of this thesis, and was a tremendous help in the project. I really enjoyed the atmosphere of the Laboratory, of which I credit my colleagues Marko Hinkkanen, Antti Piippo, and Janne Salomäki, along with other members of staff: Prof. Jorma Kyyrä, Anja Meuronen, and Ilkka Hanhivaara and former colleagues Veli-Matti Leppänen and Vesa Tuomainen, who occasionally helped me to search my inspiration, as well as a small white ball from the rough.

I also would like to thank several people in ABB, Matti Kauhanen for starting and managing this project, Juha Mikkola for his help in the laboratory, Tapio Haring for his valuable comments and enthusiasm for my research, Janne Ikonen and Tiina Tukiainen for their help especially in the DBI modification of the motor. I also thank Ilkka Erkkilä and some other less frequent participants in the project meetings. Special thanks belong to Prof. Heikki Tuusa for providing the Rogowski coils.

Finally I thank my wife Riikka for giving me the initial push to the path of academia and for her support during this journey.

Contents

List of Publications

This thesis consists of an overview and the following publications:

I   P. Mäki-Ontto and J. Luomi, "Circumferential flux as a source of bearing current of converter-fed AC machines," in *Proceedings of the 2002 IEEE Nordic Workshop on Power and Industrial Electronics, NORPIE 2002*, Stockholm, Sweden, 2002.

II P. Mäki-Ontto and J. Luomi, "Common-mode flux calculation of ac machines," in *Proceedings of the International Conference on Electrical Machines, ICEM 2002*, Bruges, Belgium, 2002.

III P. Mäki-Ontto and J. Luomi, "Bearing current prevention of converter-fed ac machines with a conductive shielding in stator slots," in *Conference Record of the IEEE International Electric Machines and Drives Conference, IEMDC 2003*, Madison, WI, 2003

IV P. Mäki-Ontto and J. Luomi, "Design of converter-fed induction motors to reduce bearing currents," in *Proceeding of the International Conference on Electrical Machines, ICEM 2004*, Cracow, Poland, 2004.

V   P. Mäki-Ontto, H. Kinnunen, and J. Luomi, "AC motor cable model suitable for bearing current and over-voltage analysis," in *Proceeding of the International Conference on Electrical Machines, ICEM 2004*, Cracow, Poland, 2004.

VI P. Mäki-Ontto and J. Luomi, "Induction motor model for the analysis of capacitive and induced shaft voltages," in *Conference Record of the International Electric Machines and Drives Conference, IEMDC 2005,* San Antonio, TX, 2005

VII P. Mäki-Ontto, H. Kinnunen, and J. Luomi, "Three-phase model for the simulation of common-mode phenomena and shaft voltages in AC motor drive systems," in *Conference Record of the International Electric Machines and Drives Conference, IEMDC 2005,* San Antonio, TX, 2005

VIII   P. Mäki-Ontto, J. Luomi, and H. Kinnunen, "Reduction of capacitive and induced shaft voltages in an induction motor drive using dual-bridge inverter approach," *Electrical Engineering (Archiv für Elektrotechnik)* (in press).

The author has written all publications with help and guidance of Prof. Luomi. The measurements and analyses for all publications were carried out by the author with the following exceptions: Mr. Kinnunen made the measurements and determined the parameters from the measurements, and took care of the circuit simulator implementation of Publication V. Publication VII is based on Mr. Kinnunen's Master's Thesis, which was partly instructed by the author. Mr. Kinnunen also made the simulations for Publication VIII.

List of Symbols

A	Area of a cross-section
C	Capacitance
C_b	Bearing capacitance
C_{sr}	Stator core-to-rotor capacitance
C_{wr}	Stator winding-to-rotor capacitance
C_{ws}	Stator winding-to-core capacitance
$\underline{H}$	Magnetic field strength
$\underline{i}_b$	Bearing current
$\underline{i}_{cm}$	Common-mode current
$\underline{i}_1$	Current flowing in a lamination
j	Imaginary unit
L	Inductance
L_c	Common-mode inductance of the stator core
L_s	Self-inductance of the stator winding
$L_{\sigma s}$	Leakage inductance of the stator winding
M_s	Mutual inductance of the stator winding
N	Number of laminations in the stator core
P_1	Losses in a lamination corresponding to $\underline{i}_1$
P_{tot}	Total (common-mode) losses in the stator core
r	Radial coordinate in cylindrical coordinates
r_1	Inner radius of the stator yoke
r_2	Outer radius of the stator yoke
R_b	Bearing resistance
R_c	Common-mode resistance of the stator core
R_1	Resistance of a lamination
R_s	Phase resistance of stator winding
S_1	Switch
$\underline{u}_{cm}$	Common-mode voltage
$\underline{u}_{sh}$	Shaft voltage
z	Axial coordinate in cylindrical coordinates
$\underline{Z}_b$	Bearing impedance
$\underline{Z}_c$	Common-mode impedance of the stator core
$\underline{Z}_d$	Bearing circuit impedance of the stator core

$\underline{Z}_g$	Grounding impedance
δ	Skin depth
μ	Permeability
σ	Conductivity
φ	Azimuthal coordinate in cylindrical coordinates
$\underline{\phi}_{cm}$	Common-mode (circumferential) magnetic flux
$\underline{\phi}_1$	Magnetic flux of a lamination corresponding to $\underline{i}_1$
ω	Angular frequency

Complex-valued variables are underlined and magnitudes of these variables are referred to by omitting the underlining.

1 Introduction

The three-phase induction motor is today the most widely used electric motor type. The induction motor can be connected directly to the mains if a constant speed is adequate for the application in question. When the induction motor is operated by means of a frequency converter, the list of possible applications becomes almost endless. Regardless of the power losses in the converter and increased harmonic losses in the motor, speed control increases the total energy efficiency in many applications. The vector control of a converter-fed induction motor has enabled high-performance torque and speed control, whose quality equals the control of dc motors. As a consequence, induction motors have largely superseded dc motors.

A continuous trend in power electronics is a shorter rise time of the pulse width modulated (PWM) voltage pulses, which reduces the losses in the power semiconductors. Consequently, the size of the converter decreases and higher switching frequencies can be used. The increased switching frequency enhances the quality of the current of the motor and decreases the harmonic losses in the motor.

However, a short rise time of the PWM voltage may also cause problems in the form of electromagnetic interference (EMI). The harmonic content of the voltages and currents is shifted to higher frequencies, possibly increasing EMI in the mains. Steep voltage pulses also pose threats to the motor. Because of the transmission line effect in the motor cable, voltage and current waves propagate at a finite velocity in the cable, and reflect from the impedance discontinuities at the motor terminals and the converter output. A superposition of the reflected voltages at the motor terminals may result in overvoltages possibly causing a failure in the stator winding insulation of the motor.

A common-mode voltage is present in the output voltage of the frequency converter. This voltage may cause bearing currents in the motor. Bearing currents generate bearing wear in forms of pitting, frosting, and spark tracks at the surfaces of the bearing balls and races (Costello 1993). The bearings may fail prematurely because of the additional friction and the polluted lubricant in the bearing.

Bearing currents are often divided to three categories: discharge currents, shaft grounding currents, and circulating currents. The distribution of the common-mode voltage between parasitic capacitances in the motor causes a capacitive shaft voltage (Chen et al. 1995). This voltage follows the waveform of the common-mode voltage, and its amplitude is determined by the ratio of the parasitic capacitances in the motor. The capacitive shaft voltage is the reason for a discharge current through the bearings.

The common-mode voltage can also cause a rise in the stator frame potential if the grounding is not sufficient. This stator potential can discharge through the bearings when the load machinery provides a low-impedance path for the common-mode current, resulting in a shaft grounding current (Ollila et al. 1997a).

Parasitic capacitances in the drive provide low-impedance paths for a high-frequency common-mode current driven by the steep edges of PWM voltage pulses. In the motor, a high-frequency common-mode current causes a magnetic field in the stator yoke (Chen et al. 1996c). This circumferential magnetic flux encircles the shaft and induces a voltage in a loop formed by the stator, the rotor, and the bearings. If the voltage exceeds the breakdown voltage of the oil films in the bearings, a circulating bearing current flows through the bearings.

The capacitive shaft voltage causes bearing damages in small motors, whereas the induced shaft voltage is considered the dominant cause of bearing failures in large motors. The limit between small and large motors in this context is vague, but the order of magnitude is a shaft height between 280 to 315 mm and a motor power around 100 kW (Link 1999, Barker 2000, Muetze and Binder 2002).

Various high-frequency circuit models of induction motors have been presented in the literature. However, only a few of these models is intended for the analysis of shaft voltages. The interest in these models has been in the capacitive shaft voltage, probably because of the small size of the investigated drives and a lack of complete understanding of the induced shaft voltage phenomenon. The shaft-encircling magnetic flux generated by the high-frequency common-mode current has so far been known only at concept level, and a rigorous model for the induced shaft voltage has not been presented. Moreover, the motor model alone is not adequate for the bearing current analysis because the common-mode voltage at the motor terminals is determined by the common-mode impedance distribution in the whole drive system. This distribution is also frequency-dependent. Therefore, the model of the whole drive system is important, especially in the simulation of the induced shaft voltage.

The bearing impedance should be modeled in order to simulate the bearing current. However, the bearing impedance is a nonlinear function of the shaft voltage (Erdman et al. 1996), and it is also affected by many other variables, for example the temperature and the mechanical load in the bearing. So, the shaft voltage is more useful as an indicator of possible bearing problems, and it is therefore exclusively investigated in the thesis. The presented model can be supplemented with a bearing impedance model if the actual bearing current is of interest.

The goals of this thesis are to develop a model of the electric drive for the simulation of both capacitive and induced shaft voltages and to investigate promising methods for bearing current mitigation in ac motors. To attain these goals, several intermediate objectives can be recognized:

- Analysis of the magnetic field that causes the induced shaft voltage

- A model for the induced shaft voltage suitable for circuit simulator implementation
- A three-phase induction motor model that includes the models of both induced and capacitive shaft voltages
- Development of the models and the parameter calculation of other drive system components
- Experimental investigation of shaft voltage mitigation methods and the model validation

Experiments and electromagnetic field calculations are carried out in order to gain a full understanding of the induced shaft voltage phenomenon. Analytical expressions are derived for the circumferential magnetic flux and the common-mode impedance of the stator core. Based on these expressions, a circuit model of the induced shaft voltage is developed and augmented with a model of the capacitive shaft voltage, and included in a three-phase model of the induction motor. The circuit models of all drive components are developed, and a complete model of the electric drive is composed. Some promising methods for bearing current mitigation in high-power low-voltage drives are investigated in the thesis using simulations, analytical expressions, and experiments. New design principles are proposed for mitigating the shaft voltages in induction motors.

The modeling of cage induction motors is exclusively discussed in the thesis. However, the presented model can be applied to any polyphase ac motor whose stator winding is fed by a frequency converter. It should also be possible to model doubly fed induction machines with minor modifications to the model. Detailed modeling of the bearings is beyond the scope of this thesis.

This thesis consists of an overview and eight publications numbered in chronological order. Chapter 2 presents the theoretical background of shaft voltages and bearing currents. Chapter 3 deals with the modeling of induction motors and other components of the electric drive. Chapter 4 reviews the methods for bearing current mitigation presented in the literature and investigated in the thesis. The laboratory setup used in the experiments is described in Chapter 5. Summaries of the publications and the scientific contribution of the thesis are presented in Chapter 6. Chapter 7 concludes the thesis.

2   Bearing Currents in AC Machines

Before the advent of the power electronics that made modern ac drives possible, various kinds of bearing current phenomena in ac machines were already known. For example, an asymmetry in the magnetic circuit of the stator was shown to cause an induced voltage in the shaft by Punga and Hess (1907), and Fleischmann (1909). The classical mechanisms causing bearing currents in machines fed from the mains are according to e.g. Ammann et al. (1988) and Kerszenbaum (1992): dissymmetry in the magnetic circuit, a homopolar flux, triboelectric effects, and an external voltage source feeding the rotor windings. The magnetic dissymmetry can be caused by joints in the laminations or rotor eccentricity. The homopolar flux may be caused by rotor eccentricity, residual magnetization, magnetic saturation, or impedance asymmetry in the stator or rotor windings. The frequency of these shaft voltages are of the order of the fundamental frequency. Triboelectric effects due to, for example, a steam brushing the turbine blades of the load machinery may cause an electrostatic discharge through the bearings. In synchronous machines, a thyristor bridge feeding the field winding in the rotor may cause currents through the bearings. It is worth noting that bearing currents generated by frequency converters may also increase the classical currents because of the low impedance of the punctured oil film in the bearing (Hausberg and Seinch 2000b).

Kerszenbaum (1992) made a statistical analysis of the bearing failures in industrial plants. Despite a relatively low number of samples, the analysis showed that bearing failures are about 12 times as common in converter-fed motors as in direct-on-line motors. Kerszenbaum drew an analogy between the classical dissymmetry-originated and converter-generated shaft voltages, which may be misleading since it was later discovered that frequency converters cause bearing currents in perfectly symmetrical machines.

It was shown by Chen et al. (1995) that the phenomenon causing bearing currents was the common-mode component in the output voltage of the converter. Chen et al. correctly identified the significance of the parasitic capacitances and the voltage divider effect in the motor that forces the shaft voltage to follow the waveform of the common-mode voltage. Examples of typical measured waveforms of the common-mode voltage and the capacitive shaft voltage are shown in Figs. 2.1(a) and 2.1(b), respectively.
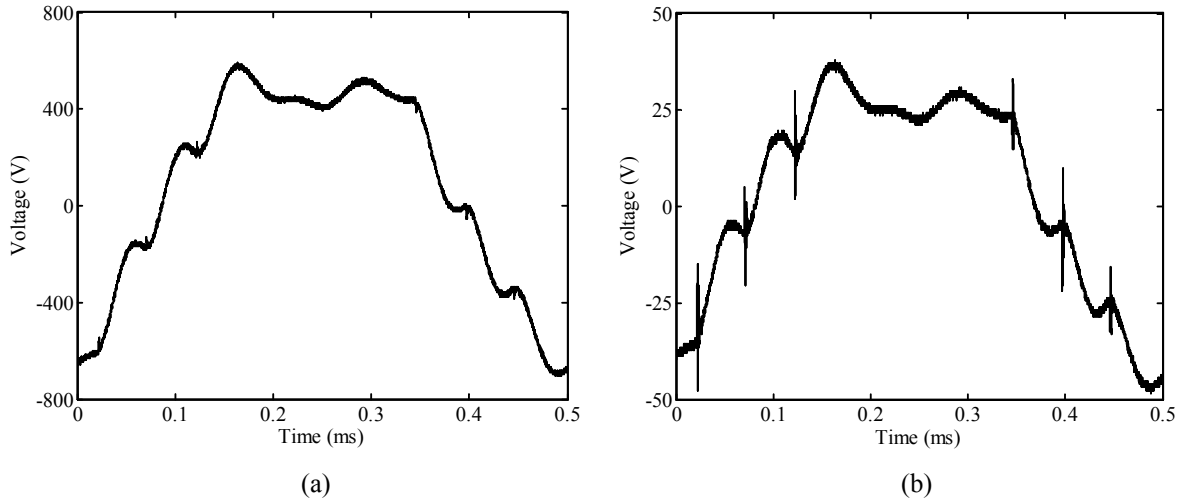
Fig. 2.1 Examples of measured (a) common-mode voltage and (b) capacitive shaft voltage.

Chen et al. (1995, 1996a, 1996b) found two types of bearing currents in their experiments: conduction mode and discharge mode bearing currents. The bearings maintain metallic contact at slow rotational speeds, and allow the current to flow through the bearings without forming a high voltage over the bearing. This conduction mode current depends on the rise time of the common-mode voltage. The path of the current is illustrated in Fig. 2.2(a), where C_{ws} is the stator winding-to-core capacitance, C_{wr} is the stator winding-to-rotor capacitance, and C_{sr} is the stator core-to-rotor capacitance. R_b denotes a low resistive impedance of both bearings, and $\underline{u}_{cm}$, $\underline{i}_{cm}$, and $\underline{i}_b$ denote the common-mode voltage, the common-mode current, and the bearing current, respectively.

At higher rotational speeds, an oil film is formed between the bearing balls and the race. Low-frequency components of the common-mode current charge the capacitance C_{sr} and the capacitance of the bearings denoted by C_b. When the bearing becomes conductive again due to a breakdown of the oil film or a contact between a bearing ball and race, a discharge current is generated, as illustrated in Fig. 2.2(b). The breakdown corresponds to closing the switch S_1. This type of bearing current does not depend on the rise time of the common-mode voltage.

The third possible bearing current mode is a capacitive bearing current (Hausberg and Seinch 2000a). A high-frequency capacitive bearing current flows through the bearing capacitance without a discharge, as illustrated in Fig. 2.2(c). Of the three bearing current types, the discharge current is the highest and the most harmful. All of these bearing current types flow to the same direction in each bearing. Erdman et al. (1996) measured the bearing resistance as a function of the rotational speed. In the investigated motor, the impedance of the bearing was approximately constant (1–10 MΩ) between the nominal speed and 10 % of the nominal speed. Below 10 %, the resistance quickly dropped to a very low value (below 1 Ω at zero speed).
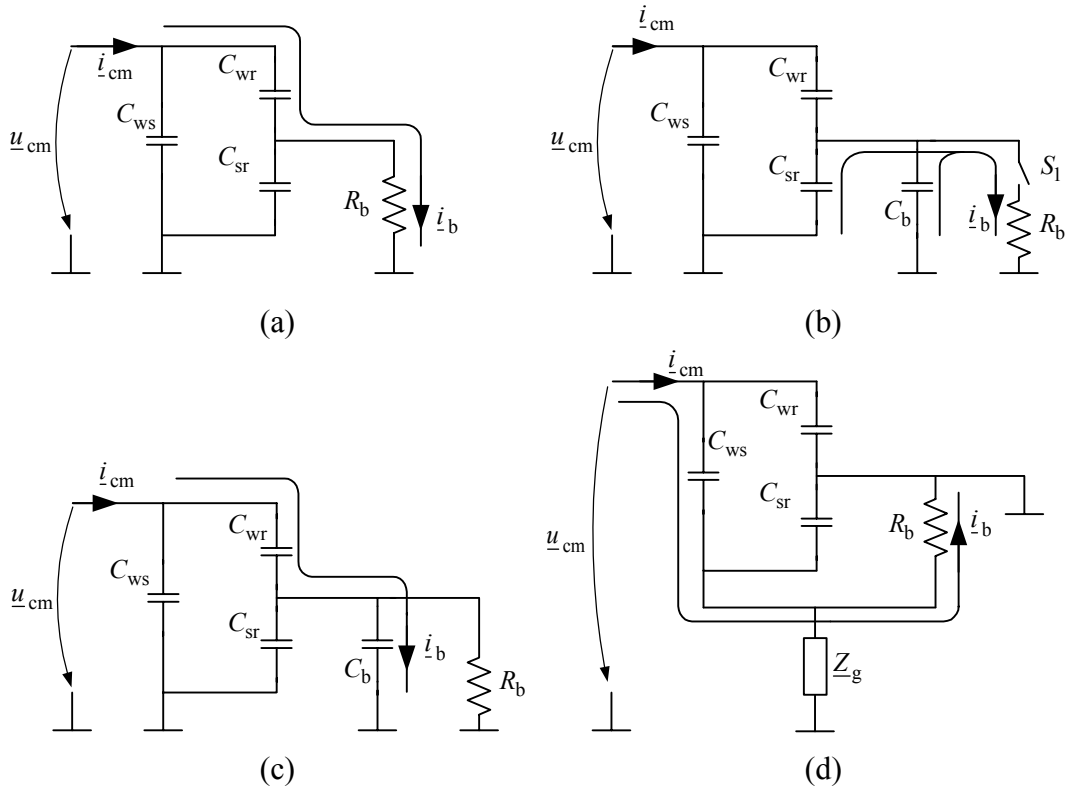
14

Fig. 2.2. Bearing current types: (a) conduction mode bearing current, (b) capacitive bearing current, (c) discharge mode bearing current, and (d) the shaft grounding current.

Ollila et al. (1997b) reported a form of bearing current that can occur if the stator frame is poorly grounded and the load machinery provides a low-impedance path for the common-mode current, as illustrated in Fig. 2.2(d). $\underline{Z}_g$ denotes the grounding impedance of the stator frame. A part of the common-mode current flows through the bearings, in practice mostly through the drive-end bearing.

Chen et al. (1996c) presented a new type of bearing current, which circulates inside the motor in a loop formed by the stator, the rotor, the end shields, and the bearings. This circulating bearing current type, illustrated in Fig. 2.3, is caused by an induced voltage between the shaft ends. The voltage is induced by a magnetic flux that encircles the shaft. Chen et al. explained the generation of the magnetic flux to be a result of the current entering the coil being higher than the one leaving the coil. The difference of these currents corresponds to an axial net current, which induces the magnetic flux around the shaft. The explanation given by Chen et al. for the induced shaft voltage is incomplete because the full path of the common-mode current should be considered in order to thoroughly explain the phenomenon, and to be able to build a circuit model for the phenomenon. Examples of the typical measured waveforms of the common-mode current and the induced shaft voltage are shown in Figs. 2.4(a) and 2.4(b), respectively. The induced shaft voltage is also visible as high-frequency spikes superposed on the capacitive shaft voltage in Fig. 2.1(b). The
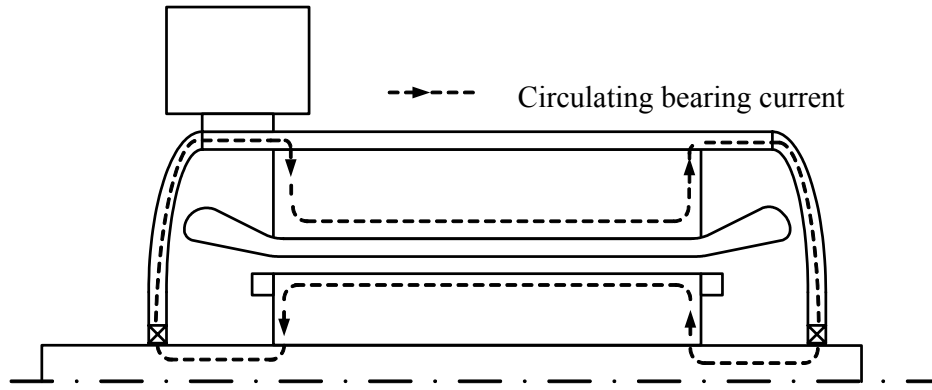
15

Fig. 2.3. The path of the circulating bearing current.

(a)

(b)
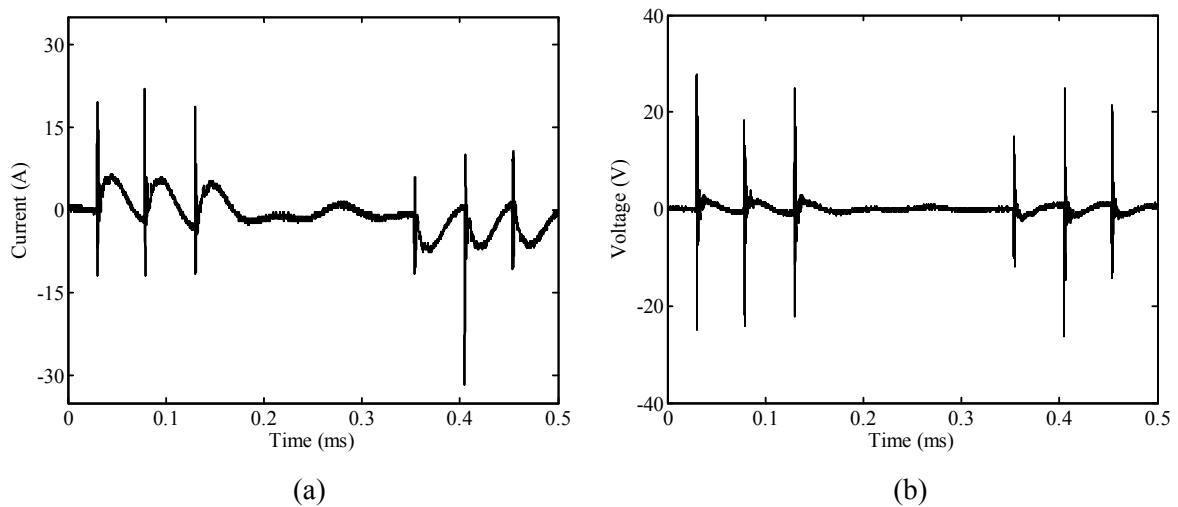
Fig. 2.4 Examples of measured (a) common-mode current and (b) induced shaft voltage.

frequencies of the common-mode current and the induced shaft voltage depend on many parameters in the system, For the analysis of induced shaft voltage, it is sufficient to consider the frequency range of 10 kHz – 10 MHz.

The distribution of the high-frequency magnetic flux in the stator core is investigated experimentally in Publication I. A 2-MW induction motor with radial cooling ducts in the stator was used in the experiment. The axial distribution of the magnetic flux was measured by search coils placed around the stator core sections. Such a flux distribution is illustrated in Fig. 2.5. According to Ampère's law, this kind of linear flux distribution is a result of an electric current reducing linearly in the axial direction. The linear reduction in the current indicates that the common-mode current density in the stator winding insulation does not vary in the axial direction and the capacitance of the winding insulation dominates in the common-mode impedance. This new observation is used in the modeling of the induced shaft voltage phenomenon (in Publications II and VI). It is to be noted that the high-frequency common-mode current cannot penetrate through the iron laminations or the stator frame because of the skin effect. Therefore, the current must flow along the surfaces of the laminations and the inner surface of the frame and hence Fig. 2.5 is only a rough illustration of the current paths.

16

Fig. 2.5. The path of the common-mode current and the distribution of the circumferential high-frequency common-mode magnetic flux encircling the shaft. The magnitude of the flux is illustrated by the size of the circles.
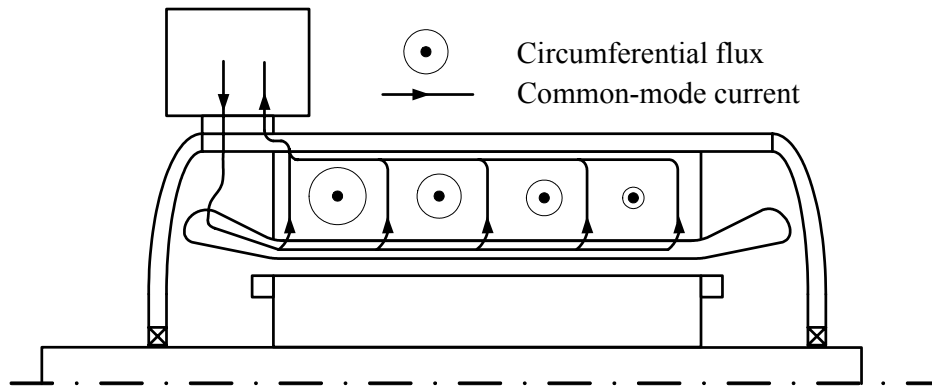
3 Modeling

Various properties are required of the induction motor model used in the analysis of shaft voltages and bearing currents. First of all, the model should be compatible with the models of the other drive system components. Therefore, a three-phase model is an obvious selection, as illustrated in Publications VI and VII. Because the common-mode voltage of the inverter causes the bearing current phenomenon, a finite common-mode impedance is needed to provide a path for the common-mode current. This impedance is capacitive in a wide frequency band due to the stator winding insulation. A physically reasonable three-phase model implicitly contains the common-mode circuit. Moreover, because relatively high frequencies are of interest, the resistances and inductances are not equal to those at the fundamental frequency. Finally, a model of the bearing circuit with the models of both capacitive and induced shaft voltages is needed.

3.1 Motor Models Presented in the Literature

Various high-frequency models of induction motors have been presented in the literature. Schlegel et al. (1999) demonstrated how the power, the frame size, and the vendor of the motor affect the measured differential-mode impedance in a frequency band of 20 Hz – 1 MHz. The use of separate circuits for the differential and common modes was proposed by Consoli et al. (1996). These equivalent circuits consisted of a minimal number of components. The number of reactive components was selected so that the model produces the same number of critical frequencies as was detected in the measurements. The values of the inductances and capacitances were determined from the slopes and the critical frequencies of the measured admittance curves, and the resistances were adjusted for correct damping at the critical frequencies. Dolezel et al. (2000) presented a similar model that consists of several LC circuits in series to represent the nonlinear voltage distribution in the coils. Boglietti and Carpaneto (1999) suggested a pi-equivalent circuit model for the common-mode impedance. The parameters of the circuit were determined from measurements of parallel-connected open- and short-circuited winding phases. In the revised version of their model, Boglietti and Carpaneto (2001) added a simple skin effect model to the model.

Ahola et al. (2003) made a series of impedance measurements to induction motors of powers between 15 kW and 250 kW in a frequency band of 10 kHz – 30 MHz. They proposed that the investigated motors be modeled by parallel resonance circuits for the differential mode and series resonance circuits for the common mode. They also measured the impedance

of a 15-kW motor with and without the rotor and end shields and found out that the effect of the rotor and end shields on the high-frequency impedances is low.

Because the differential- and common-mode impedances are not modeled simultaneously in the same model, the previously mentioned models are not suitable for the simulation of a converter-motor combination. A three-phase induction motor model containing both differential- and common-mode behavior was presented by Grandi et al. (1997). The parameters of the model were determined from impedance measurements, and the model is suitable for both differential-mode and common-mode conducted EMI analysis.

Chen et al. (1995) published the first common-mode equivalent circuit model able to predict the capacitive shaft voltage. The model is illustrated in Fig. 3.1. The parameters of this model were identified from measurements with a 3-hp induction motor. The parameter calculation of this model was further developed by Busse et al. (1997d). Cacciato and Testa (2000) presented a three-phase high-frequency model of an induction motor, which also includes the model for the capacitive shaft voltage. Naik et al. (2003) presented a model that can be added in parallel with a fundamental-frequency three-phase motor model. The model represents the common-mode impedance of the motor in a wide frequency band and also includes the capacitive shaft voltage calculation. Busse et al. (1997b) proposed a circuit model for the bearing suitable for the bearing current analysis.

Despite a large number of presented models, the induced shaft voltage phenomenon is not modeled in any of these models. Moreover, a model based on the geometry of the motor has not been presented (instead of impedance measurements followed by an identification of the model parameters).

3.2 Numerical Analysis of the Common-mode Magnetic Field

A formulation of Maxwell's equations suitable for the simulation of the high-frequency electromagnetic field in the stator laminations is derived in Publication II. The following assumptions and simplifications are made in the modeling:

- The magnetic field is assumed to be concentrated in the stator yoke and frame, i.e. the teeth are excluded from the model and the stator core is approximated by a cylinder, as illustrated in Fig. 3.2. The magnetic field problem is formulated as rotationally
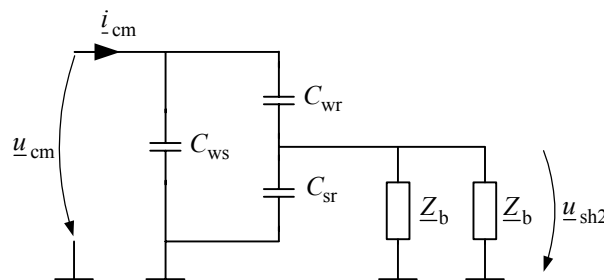

Fig. 3.1. Model of capacitive shaft voltage (Chen et al. 1995). The impedance of each bearing is denoted by $\underline{Z}_b$ and the capacitive shaft voltage is denoted by $\underline{u}_{sh2}$.
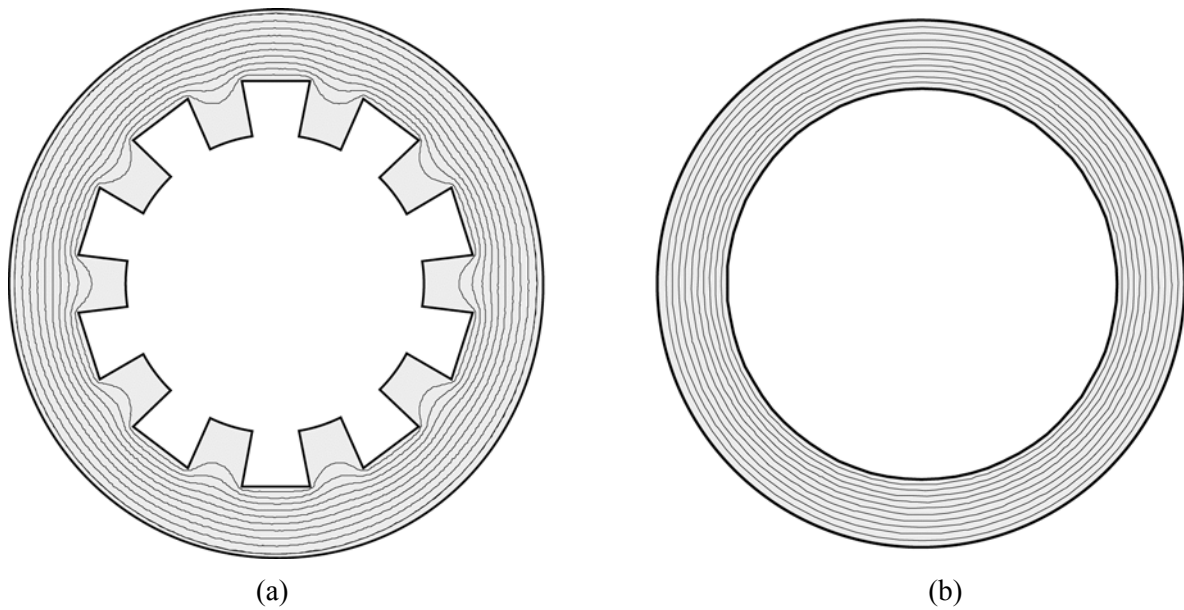
20

Fig. 3.2. Illustration of the effect of the slotting on the high-frequency magnetic field in the stator: flux lines (a) slotted stator, (b) stator approximated with a cylinder.

symmetric using only the azimuthal component of the magnetic field strength. The high-frequency common-mode current cannot flow through the massive iron frame covering the stator core. Therefore, it is reasonable to assume that the magnetic field is zero outside the motor. The thickness of the stator winding insulation in the model is selected so that the capacitance is equal to the original capacitance between the stator winding and the core. Because of the ratio of the parasitic capacitances, only a small part of the common-mode current flows in the rotor. Therefore, the rotor is not included in the model. Muetze et al. (2005) have later investigated the effect of the slotting on the high-frequency circumferential flux. They found the effect to be the most significant in machines with high number of poles because of lower yoke height. They also suggest a correction (discrepancy) factor, whose value depends on the motor geometry.

- The common-mode current is too small to alone saturate the stator core. The high-frequency magnetic field is biased by the periodic distribution of the rotating fundamental-frequency magnetic field. Therefore, an incremental permeability is used in the analysis of this field. The incremental permeability varies along the circumference, and this permeability distribution rotates at the fundamental frequency. The incremental permeability has its maximum value in the case of zero biasing flux density, and it approaches the permeability of vacuum μ_0 with magnetic saturation (Bozorth 1993). A constant value of the incremental permeability is used for the analysis of the circumferential magnetic flux.

- The conductivity of the insulation between the core laminations is assumed zero in the analysis, whereas the permittivity of the insulation is taken into account. The effect of

the lamination insulation on the common-mode impedance and the circumferential magnetic flux was investigated by means of circuit models as described in Section 3.3, showing that it is negligible in the frequency band of interest.

- At low frequencies, the differential-mode voltage decreases linearly from the terminals to zero at the star point of the winding, whereas high-frequency components of the voltage are concentrated over the first turns of the winding. The common-mode voltage, however, seems to behave differently. Fröberg (2003) measured the common-mode voltage and the star-point voltage simultaneously in a 250-kW drive. The difference between these voltages was small. Furthermore, the measured linear flux distribution presented in Publication I indicates that the common-mode current density in the stator winding insulation does not vary in the axial direction. Therefore, it is assumed that the common-mode voltage is constant in the stator winding.

An example of the finite element method (FEM) solution of the formulation is shown in Fig. 3.3. The magnetic field and the common-mode current are illustrated in five 0.5 mm thick iron laminations. The stator frame is grounded at the left-hand side of the frame, and the common-mode current density is constant at the surface of the stator winding. The other dimensions and the relatively low frequency of 30 kHz are selected for visual clarity in this example. The field lines would be nearly indistinguishable from the geometry lines at relevant frequencies (about 1 MHz) since the skin depth in the core material is of the order of 10 μm. It follows from the boundary conditions that the flux outside the motor is zero. Because of the skin effect, the common-mode current returns to the grounding along the surfaces of the laminations, and the current flowing in the rightmost lamination flows through each lamination to the grounding. The magnetic flux has a maximum value in the lamination near the grounding, and the flux decreases lamination by lamination linearly from left to right. The field solution illustrates the fact that the circumferential magnetic flux and the common-mode current are not separate but just two manifestations of the same field. It is to be noted that if the stator frame would be grounded at the right-hand side of the frame, the common-mode current would continue from left to right along the outer surface of the frame.

The results of Publication II are in line with the measurement presented in Publication I. The magnetic field simulation of the whole stator core is too laborious since the core consists of hundreds or thousands of iron laminations. Therefore, simpler models are needed. Analytical expressions of the circumferential flux and the common-mode impedance of the core are presented in Publication II. These expressions are used as a starting point for the circuit model of the induced shaft voltage phenomenon as described in the next Section.
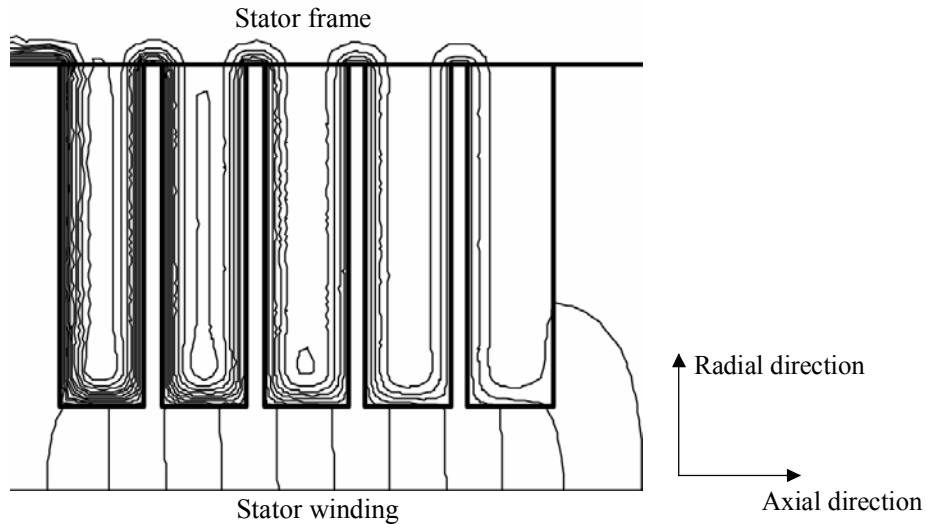
Fig. 3.3. Contour plot of magnetic field strength (corresponding to equal currents between curves) in winding insulation and five iron laminations.

3.3 Circuit Model

The skin depth is much smaller than the iron lamination thickness in the frequency band of interest for the shaft voltage analysis. Therefore, the electromagnetic field at each lamination surface can be modeled by a plane conductor of infinite depth in the axial direction. The current also flows in the axial direction at each end of lamination and also in the frame, as can be seen in Fig. 3.3. However, the contribution of this current in total flux is negligible in a real machine because of the small ratio of the lamination thickness to the yoke height. Analytical expressions are given for the circumferential flux and the common-mode impedance of the stator core in Publication II. The derivations of these expressions are presented in Appendix I. Figure 3.4 illustrates the equivalent circuit corresponding to the expression for the common-mode impedance. The contribution of each iron lamination on the total common-mode impedance is included in the resistance R_c and the inductance L_c, which are frequency-dependent.

Fig. 3.4. The equivalent circuit representing the stator winding capacitance and the core impedance.

Publication VI deals with circuit models of the induced shaft voltage phenomenon. Since the common-mode current and the corresponding magnetic flux flow at the surfaces of the laminations, each lamination surface can be modeled by an impedance of a layer whose thickness equals the skin depth. A detailed model of 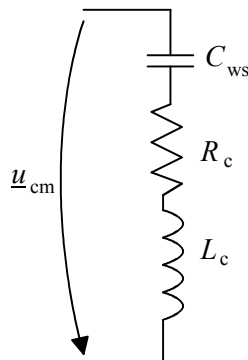the common-mode circuit is depicted in Fig. 3.5. The terminals of the winding and the grounding are at the leftmost end of the core. It is assumed that the electric potential of the stator winding is equal to the common-mode voltage $\underline{u}_{cm}$ (Node 1). The stator winding capacitance is subdivided into smaller capacitances C, and the common-mode current $\underline{i}_{cm}$ flows to individual laminations through these capacitances. The induced shaft voltage $\underline{u}_{sh1}$ is the potential of Node $N+2$ in the circuit. The circulating bearing current is denoted by $\underline{i}_{b}$. The bearing circuit is modeled by a series connection of two bearing impedances $\underline{Z}_{b}$ (which also include the impedances of the end shields and the rotor). The insulation impedances between adjacent laminations are assumed infinite. The effect of these impedances on the common-mode impedance and circumferential magnetic flux is analyzed in Appendix II. According to this analysis, the lamination insulation has no significant effect below the frequency of 1 MHz, and its effect is of minor importance even at higher frequencies.

Possibilities of model reduction are also investigated in Publication VI. In the reduced model illustrated in Fig. 3.6, the core is subdivided into sections, and equal current is assumed to enter each lamination within each section. Thus, the impedance of each section can be calculated using the expression given in Publication II for the whole core. If equal current is assumed to enter each lamination in the whole core, the common-mode circuit and the bearing circuit can be modeled by a simple circuit model, illustrated in Fig. 3.7. In the case of zero current in the bearing circuit, this model is equal to the model shown in Fig. 3.4. The induced shaft voltage cannot be obtained as a node potential in the simple model, but suitable voltage controlled voltage sources are employed for taking the induced voltages into account correctly. The induced shaft voltage is generated by the voltage source $\frac{3}{2}\underline{u}_{1}$ in a separate bearing circuit, and the influence of the circulating bearing current on the common-mode circuit is taken into account by means of the voltage source $\frac{1}{2}\underline{u}_{2}$.

A lower frequency limit of approximately 10 kHz can be given for the validity of these models if the skin depth of the core material is restricted to values lower than one tenth of the lamination thickness. In most cases, this limit is not relevant: due to the stator winding capacitance, the common-mode impedance is high at frequencies below 10 kHz, and the common-mode current is practically zero. The upper limit of the frequency depends on the selected core model.

Because of the skin effect, the core impedances depend on the frequency. A core model suitable for time-domain simulations is obtained by modeling the frequency-dependence of the core impedances by means of ladder circuits proposed by Yen et al. (1982). A method presented by Kim and Neikirk (1996) can be applied for determining the suitable resistance
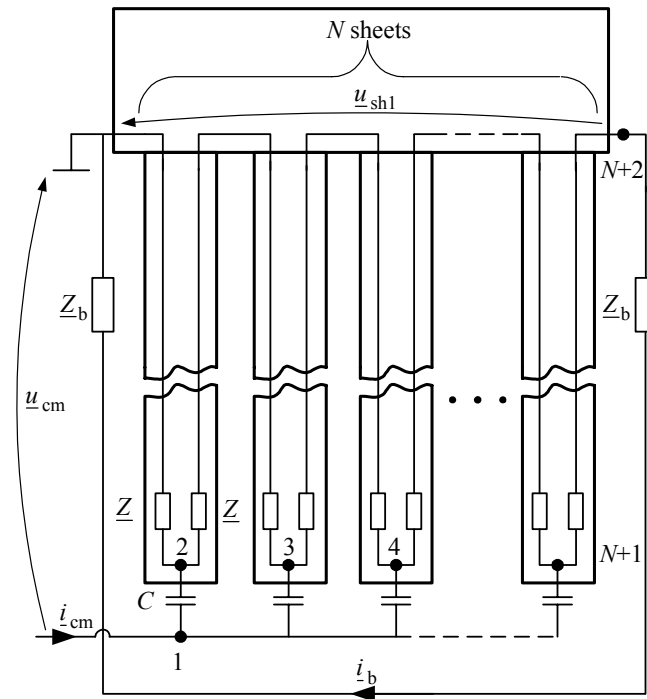
Fig. 3.5. Detailed core model
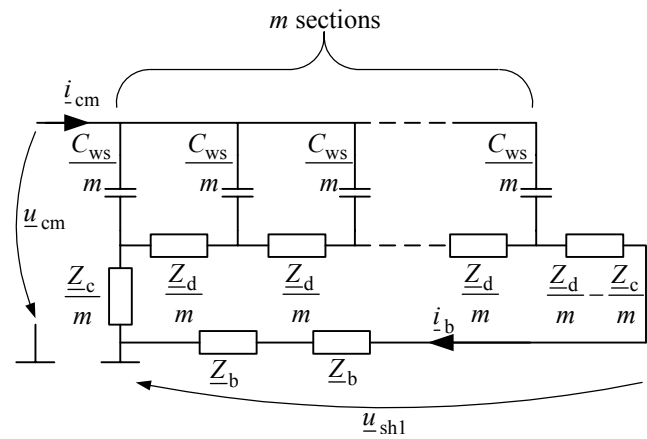
Fig. 3.6. Reduced core model

Common-mode circuit   Bearing circuit
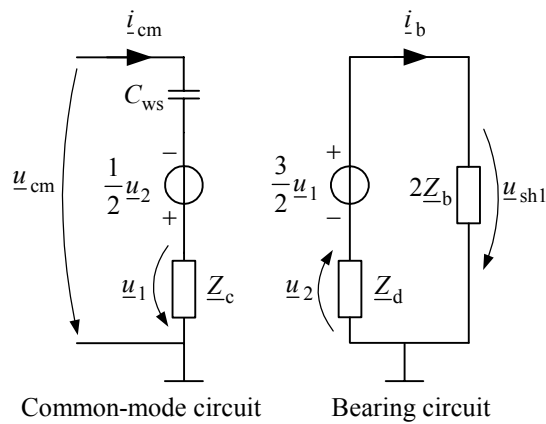
Fig. 3.7. Simple core model

and inductance values of the ladder circuit. Publication VI proposes a three-phase model of induction motors that includes the models of both capacitive and induced shaft voltages. The complete model developed in Publication VI is illustrated in Fig. 3.8. A three-phase model suitable for circuit simulation (Pillay and Levin 1995) is used for the stator winding, and the model of Chen et al. (1995) is used for the capacitive shaft voltage.

Compared to the models presented in the literature, the motor model is unique in two ways: the model is able to predict the induced shaft voltage in addition to the capacitive shaft voltage, and the components of the model have physical meaning. The model was validated by comparing simulations and laboratory measurements. The waveform and the amplitude of the simulated induced shaft voltage corresponded very accurately to the measurement. Even though the model is based on the motor geometry, measurements are needed in the determination of the value of the incremental permeability. The model can be further improved by adding a skin-effect model for the stator winding resistance and leakage reactance.
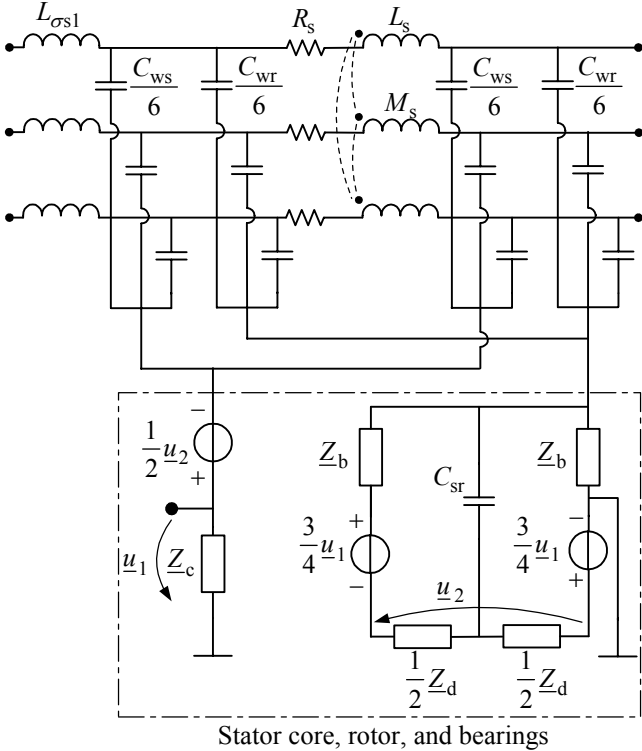
Fig. 3.8. Three-phase motor model including the combined shaft voltage model.

3.4   Models of the Other Drive System Components

For bearing current analysis, it is essential that the common-mode voltages and currents at the motor terminals can be predicted with a sufficient accuracy. If the common-mode voltage at the inverter output is accurately known a priori, it is possible to use a model consisting merely of the common-mode impedances of the drive system (Busse et al. 1997d). A typical electric drive consists of the power grid, the converter, the motor, and the cables. All these components have a contribution to the common-mode impedance. The possible paths of the common-mode current are depicted in Fig. 3.9. The common-mode current generated in the inverter is denoted by i_1 in the figure. The current i_2 branches off to the leakage capacitances of the cable and the remaining current i_3 flows through the motor. These currents are again summed up in the protective earth conductor of the cable. A part of the current, i_5, flows through the parasitic capacitances between the inverter cabinet and the dc buses, and the rest of the current, i_6, returns to the inverter through the power grid.

The effect of the power grid on the common-mode impedance depends on the grounding conditions. Hyypio (2005) demonstrated that a distinctive reduction is obtained in the common-mode voltage at the motor terminals when the neutral of the supply transformer secondary winding is isolated from the ground. A 15-hp motor and 43-kVA converter were used in the experiments. The common-mode current distribution in a 1.4-MW motor and a 1160-kVA frequency converter presented in Publication VII also suggests that the power grid provides a significant path for the common-mode current to flow. Complicated models of the power supply should be avoided because the determination of the model parameters is difficult. A simple equivalent circuit for the power supply is proposed in Publication VII.

A model of frequency converter is needed to produce the phase voltages and the resulting common-mode voltage. The semiconductor components forming the switches can be modeled using various methods (Sheng et al. 2000). The most important property of the switch model is the correct rise time of the voltage. Ideal switches are not advisable, as the rise time is determined by the time step used in the calculation. Commercial circuit simulators usually include generic models of IGBTs or even model libraries of IGBT manufacturers. The rise time is independent of the time step in such models, as long as the time step is shorter (preferably an order of magnitude) than the rise time. A generic IGBT model included in the Simplorer circuit simulation software was used in Publication VII. The parameters of the IGBT were obtained from the datasheets of the manufacturer. The converter also includes parasitic inductances and capacitances. It was shown in Publication VII that the leakage capacitance of the converter has a significant effect on the common-mode current of the motor, even though this capacitance is very small compared to e.g. the leakage capacitance of the motor.

The motor cable affects the common-mode current of the motor because a part of the common-mode current returns to the inverter via the cable capacitances. A long cable cannot
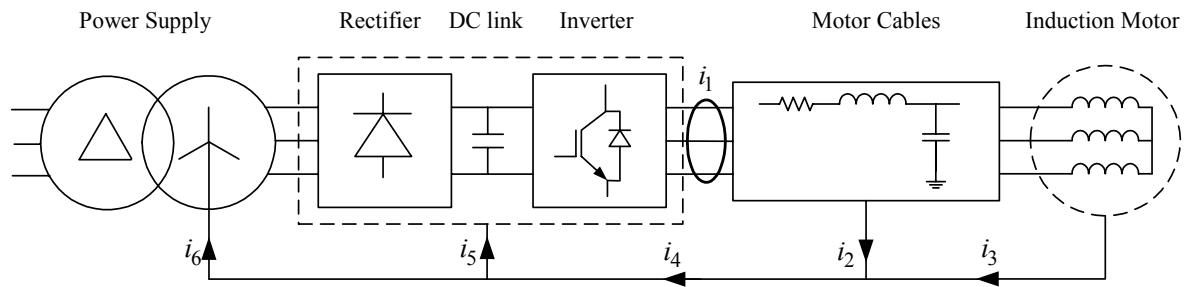
Fig. 3.9. The paths of the common-mode current in a typical drive system.

be modeled by lumped parameters because of the transmission line effect. The capacitance and the inductance of the cable determine the propagation velocity of the traveling waves, and the resistance determines the damping. Therefore, it is important that the parameter values are correct. Cable models are discussed, e.g., by von Jouanne et al. (1995), Hussein and Joos (1997), Skibinski et al. (1998), Hofmann (2003), and Moreira et al. (2001).

The cable resistance increases and the cable inductance decreases when the frequency increases. Constant high-frequency values are not applicable since the impedance of the cable would be too high at lower frequencies, and the terminal voltage of the motor would be extremely distorted due to the voltage drop over the cable. A physical cable model including frequency dependent parameters was presented by Tellinen (1999). An additional problem is encountered when the cable behavior is to be modeled for both differential-mode currents and common-mode currents since these currents cause different magnetic field distributions. The common-mode resistance of the phase conductors is higher and the internal common-mode inductance is lower than the corresponding differential-mode quantities. It is shown in Publication V, however, that a sufficient accuracy can be achieved for both differential-mode and common-mode phenomena if the frequency-dependent parameters of the cable model are calculated for the common-mode case.

Publication VII compares results of system simulations to measured results. The model predicts waveforms, frequencies, and amplitudes of common-mode voltages and currents in the drive system with a good accuracy. The model was also tested by adding a filter to the system. Also in this case, the simulation results and the measurement results were in good agreement.

The inclusion of all the details of the drive system may result in a very large model. A frequency converter may consist of many parallel inverter units and a switch may consist of many parallel IGBTs. Parallel motor cables may be also employed in a drive system. The reduction of the number of parallel components is investigated in Publication VII. A system of two parallel inverter units, 36 IGBTs, and four motor cables is reduced to a system with six IGBTs and one cable without sacrificing the accuracy of the results.

4   Methods for Bearing Current and Shaft Voltage Mitigation

Various methods have been discussed in the literature for the mitigation of shaft voltages and bearing currents. Modifications can be made in the motor for increasing the impedance in the bearing circuit or for completely avoiding the shaft voltage. The common-mode voltage and current generated by the converter can be reduced by passive or active filters. The common-mode voltage can be reduced or even canceled by special converter topologies or modulation techniques. In the following, a review of these methods is presented.

4.1   Motor Modifications

Some basic motor modifications (e.g., carbon brushes and bearing insulations) developed against the classical bearing currents are still in use for the mitigation of converter-generated bearing currents. Carbon brushes are used for grounding the rotating shaft and shunting the bearing current to the ground. A drawback of the carbon brush is that a motor equipped with a brush needs more maintenance. Bearing currents can be prevented by bearing insulations embedded in the end shields, or by hybrid bearings with ceramic rolling elements. It is to be noted that bearing insulations working perfectly against classical bearing currents may not be adequate for high-frequency bearing currents caused by frequency converters. Thin insulation forms a capacitance whose impedance at high frequencies may be too low to reduce the current to an acceptable level. A drawback of hybrid bearings and bearing insulations is that the unwanted shaft voltage remains and may endanger the bearings of the load machinery or the pulse encoder, or the voltage may cause a risk of sparks and explosion in a hazardous environment. Conductive lubricants have also been proposed as a cure for the shaft voltage build-up. However, such products with adequate lubrication properties are not commercially available.

Adding an electrostatic shield inside the motor has been proposed for a reduction of the capacitive shaft voltage. The purpose of the shield is to break the capacitive coupling between the stator and the rotor as illustrated in Figs. 4.1(a) and 4.1(b). Busse et al. (1997c) suggested three different shield designs: a copper foil that spans over the whole stator-side air-gap surface; copper-plated stator slot sticks connected together in one end of the motor; and the stator core and end windings sprayed with a conductive copper paint. The common denominator for these shield configurations is that they are all insulated from the stator core and the shield is grounded at one end of the motor. Busse et al. tested these shield constructions, and found that they all attenuated the capacitive shaft voltage by more than

90 %. The effect of the shield on the total losses of the motor was examined by means of temperature rise tests with three motors employing the proposed shield designs. No significant differences were noticed in the temperature rises. The shield based on copper-plated slot sticks should have the lowest losses because the fundamental-frequency flux induces the smallest eddy currents in this kind of shield. In the examined 15-hp motor, it was found that the shielding of the stator end windings is important for a good shielding effect. Kim and Nam (2000) proposed a shield consisting of an insulated conductor fitted in each stator slot opening, each conductor being grounded at one end of the motor. The attenuation of the shaft voltage was 66 % in the examined 5-hp motor. The end windings were not shielded, which probably explains the only moderate shielding effect compared to that of Busse et al.

While the electrostatic shield appears to be an adequate solution to the capacitive shaft voltage problems, it has no effect on the induced shaft voltage. Schüren (2001) proposed a different kind of shield, which reduces the induced shaft voltage. This shield covers the whole surface of the stator slot, as illustrated in Fig. 4.2(c), and provides a low-impedance path for the common-mode current, which would otherwise penetrate the stator core and cause a circumferential magnetic flux. The losses and the shielding effectiveness are investigated in Publication III. It is shown that the losses generated in the shield due to the fundamental-frequency slot leakage flux can be reduced by selecting a thinner shield or by subdividing the shield into several strips. The effect of the shield thickness on the attenuation of the common-

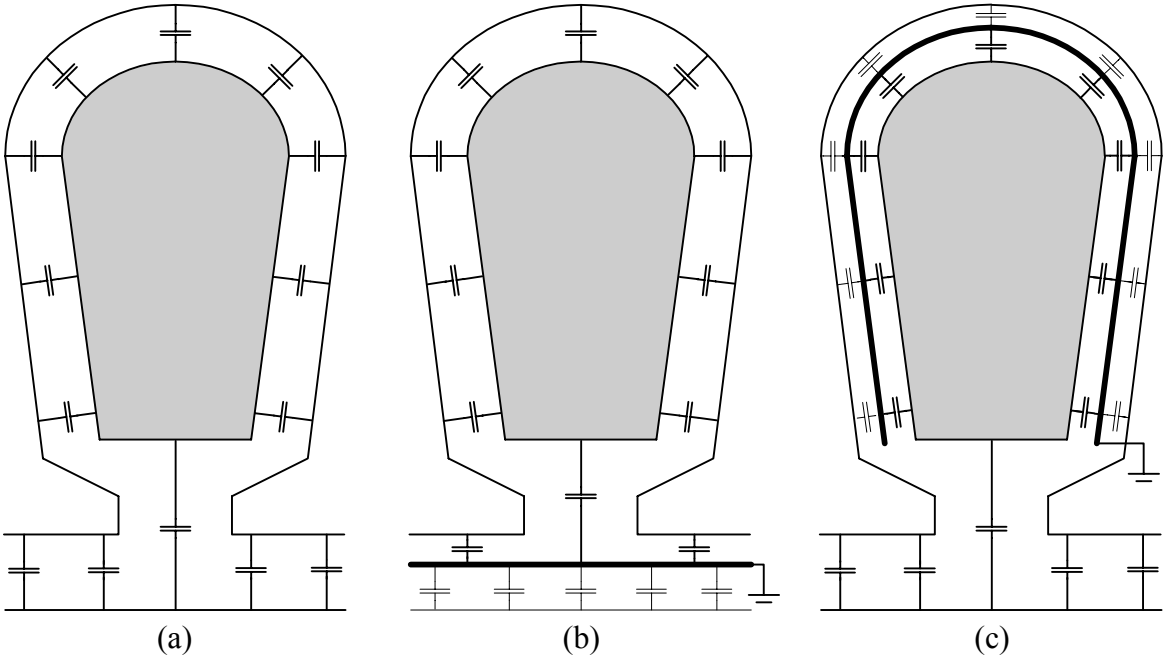| (a) | (b) | (c) |

Fig. 4.1. Shield configurations: (a) stator slot without a shield; (b) shield against capacitive shaft voltage; (c) shield against induced shaft voltage. The reduced capacitive coupling is depicted by thin lines.

mode current in the stator core is investigated using a simple equivalent circuit. A 0.01 mm thick copper shield was found to be adequate for the shielding of the 800-kW induction motor investigated. According to the analysis, the shield damps the common-mode current in the stator core over 60 dB in the investigated frequency range of 10 kHz – 1 MHz.

The bearing currents depend on the motor dimensions and the motor design. In Publication IV, new design principles are proposed for ac motors to reduce the bearing currents. A qualitative analysis is made using the dimensions of a large number of motors obtained from a motor manufacturer. The analytical expressions of Publication II are used in the analysis. According to the analysis, the most significant parameter is the diameter-to-length ratio of the core. Figure. 4.2 shows the induced shaft voltages of the examined four- and six-pole induction motors as a function of the core volume. The different shaft heights are depicted as separate curves. Increasing the shaft height without changing the core volume will reduce the induced shaft voltage, as can be seen, for example, at the core volume of 0.67 m^3 in Fig. 4.2(b). As the nominal frequency can be varied, the number of poles is also a parameter to be selected. Increasing the number of poles usually results in a shorter machine, a larger air gap diameter, and a lower yoke. All of these changes will decrease the circumferential flux and the resulting induced shaft voltage.

4.2 Passive Filters

Passive filters are used in electric drives to reduce overvoltages at the motor terminals, the EMI, and the common-mode current. For the reduction of the overvoltage, von Jouanne et al. (1996) proposed a shunt filter to be placed at the motor terminals. The purpose of this filter is to balance the impedance discontinuity between the cable and the motor, thus reducing the reflected voltage wave. In the experiment made with a 3-hp motor and a 50-ft cable, von Jouanne et al. discovered that a simple first-order filter consisting of a series connected

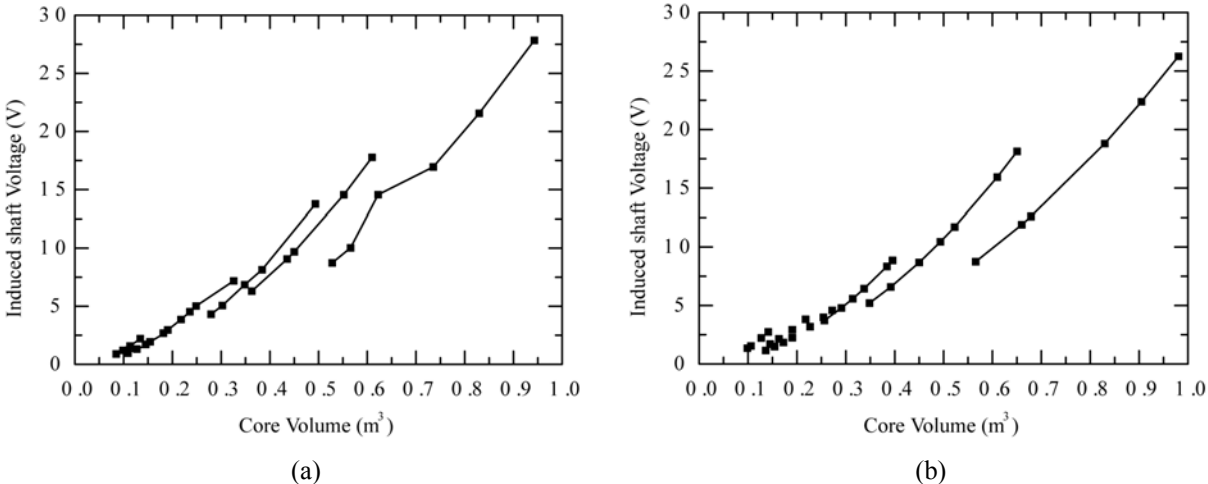(a)   (b)

Fig. 4.2. A qualitative analysis of induced shaft voltage in (a) four- and (b) six-pole induction motors as a function of the core volume. A common-mode voltage of 5 V and 1 MHz is used as a source in each case.

capacitor and resistor between the phase and ground was the most effective solution. The overvoltage at the motor terminals was totally damped, and the rise time of the voltage was almost doubled.

According to von Jouanne and Enjeti (1997), another way to reduce the overvoltages is by reducing the rate of change of the inverter output voltage. For this purpose, a conventional LCR low-pass filter shown in Fig. 4.3(a) was placed at the converter output. The converter output filter has an advantage over the motor terminal filters in such drives where the motor terminals are not accessible. In the paper, a concept of the critical rise time of the cable was introduced. It depends on the cable length, the propagation velocity of the voltage pulse in the cable, and the reflection coefficient of the cable and motor combination. The critical rise time is used in determining the cutoff frequency of the filter. The effectiveness of the concept was demonstrated experimentally in a drive consisting of a 5-kVA frequency converter, a 5-hp motor, and a 100-ft cable. In the experiment, the inverter output filter was compared with a motor terminal shunt filter. Both filters reduced the overvoltage effectively. However, the inverter output filter performed better in the reduction of the rate of change in the motor terminal voltage. Similar results were presented by Moreira et al. (2005). They recommended an LCR filter in the converter output for overvoltage reduction. According to Moreira et al., this type of filter reduces the overshoot of the voltage at the motor terminals and also increases the rise time of the voltage, smoothing the internal voltage distribution of the motor.

Rendusara and Enjeti (1998a) proposed an improvement to the conventional LCR low-pass filter by connecting the neutral point of the filter to the midpoint of the dc link, as illustrated in Fig. 4.3(b). This kind of filter effectively reduces the rate of change of both differential-mode and common-mode voltages. The cutoff frequency of the filter was selected according to the critical rise time of the cable, as suggested by von Jouanne and Enjeti (1997). The rate of change of the differential-mode voltage was reduced from 3000 V/μs to 120 V/μs, and the shaft voltage was reduced from 864 mV to 234 mV (RMS) in a 20-hp drive.

Fig. 4.3(c) illustrates a filter topology presented by Rendusara and Enjeti (1998b) for a converter with a PWM rectifier. According to Rendusara and Enjeti, the rate of change in the voltage at the terminals of a motor fed by this kind of converter may be twice as high as that caused by a converter with a diode rectifier. LCR filters are employed both at the input and the output of the converter. The neutral points of both filters are connected to the midpoint of the dc link. Experiments made with a 20-hp drive showed a significant reduction in the rate of change of the differential-mode voltage (from 2350 V/μs to 100 V/μs) and in the induced shaft voltage (from 1.456 V to 0.56 V (RMS)).

The midpoint of the dc link is not available in the case of a single dc-link capacitor or any odd number of dc-link capacitors in series. This deficiency is avoided by the filter topology in Fig. 4.3(d) proposed by Palma and Enjeti (2002). Six resistors and capacitors are used in the LCR filter, and the resulting two neutral points are connected to the positive and the negative

dc buses, respectively. This filter reduced the common-mode current by 43 % in the investigated 20-kW induction motor drive.

For the common-mode current reduction, Murai et al. (1992) proposed an LC low-pass filter whose neutral point is connected to the ground level of the dc source, which was the negative dc bus in the investigated converter. Moreover, six clamping diodes were used in the dc link, as shown in Fig. 4.3(e). The filter practically canceled out the common-mode current of the investigated 0.75-kW induction motor drive.

Habetler et al. (2002) proposed another modification to the conventional LCR low-pass filter. In this filter topology, shown in Fig. 4.3(f), clamping diodes are used in controlling the rate of change in the voltage. Because the purpose of the filter is not to filter the harmonics but to reduce the rate of change of the voltage, the resonance frequency can be higher than the switching frequency of the inverter. A considerable reduction of the rate of change on the voltage, from 2000 V/μs to less than 200 V/μs, was obtained in the investigated 20-hp induction motor. Moreover, the voltage overshoot at the motor terminals was reduced from 600 V to less than 200 V.

Hanigovszki et al. (2004) presented another filter based on the diode clamping. In this filter, shown in Fig. 4.3(g), the clamping diodes are placed in series between the dc buses, and the neutral point of the LCR filter is connected between the diodes. In the simulations and experiments shown in the paper, the diode clamp considerably enhanced the performance of the LCR filter in a 2.2-kW drive.

In a filtering scheme presented by Akagi and Doumoto (2004), the star point of the motor winding is connected to the dc buses of the converter by a resistor and two capacitors, as shown in Fig. 4.3(h) Moreover, a common-mode choke with a minimal differential-mode inductance and three differential-mode chokes are used in the output of the converter. The method is applicable only to motors with a star-connected winding, which is often not the case in large motors. The effectiveness of the filter was verified using a 5-kVA laboratory system. The filter reduced the carrier-frequency component of the common-mode voltage at the motor terminals to 4 % of the original one.

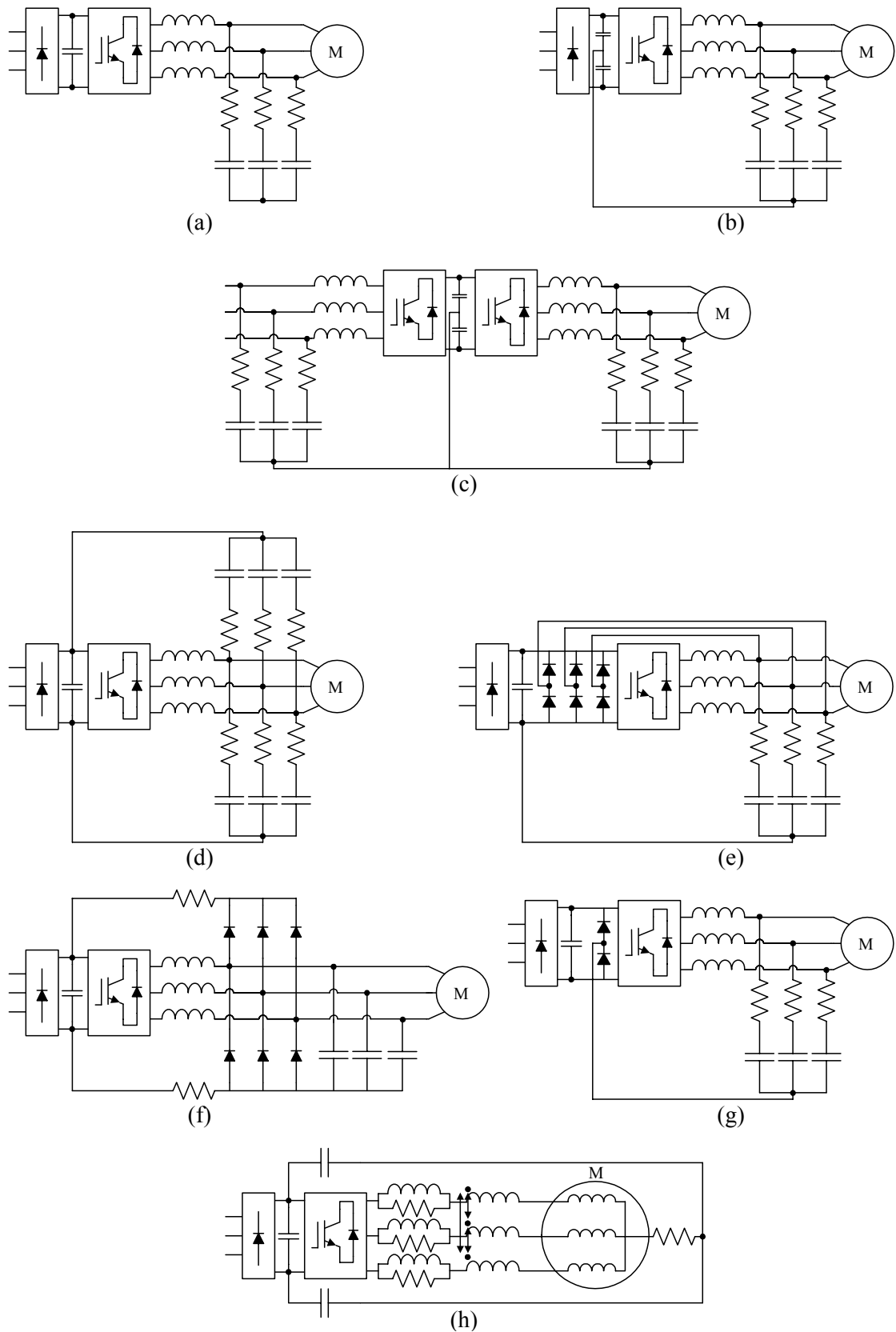Fig. 4.3. LCR output filter and its modifications: (a) conventional LCR filter; (b) neutral point grounded to dc-link midpoint; (c) filters in both input and output of PWM rectifier; (d) neutral points connected to each dc bus; (e) diode clamp filter with six diodes; (f) modified diode clamp filter with six diodes; (g) LCR filter with two clamp diodes; (h) motor neutral point connected to dc-link midpoint.

Murai et al. (1992) presented a filter based on a common-mode transformer whose primary winding consists of the three phase conductors so that the common-mode current generates a flux that induces a voltage to the secondary winding. The grounded secondary winding is fed from an artificial neutral point formed by three RC circuits, as depicted in Fig. 4.4(a). Ogasawara and Akagi (1996) used a damping resistor in the (floating) secondary winding of the common-mode transformer. This filter is illustrated in Fig. 4.4(b). The filter reduced the common-mode current of a 3.7-kW motor from 1.9 A to 0.1 A. Swamy et al. (2001) proposed the artificial neutral point to be formed by inductors instead of RC circuits. In the proposed filter, illustrated in Fig. 4.4(c), the secondary winding of the common-mode transformer was connected between the dc-link midpoint and the artificial neutral point. Swamy et al. (2001) also proposed a damping resistor to be placed in parallel with the secondary winding to reduce the size of the transformer.

4.3   Active Filters and Modulation Techniques

An active common-mode voltage canceller employing the common-mode transformer was proposed by Ogasawara and Hideki (1998). An emitter-follower, controlled by the common-mode voltage obtained using an artificial neutral point, connects the dc-link voltage in the secondary winding in order to compensate the common-mode voltage at the motor terminals, as depicted in Fig. 4.4(d). Xiang (1998) proposed a similar active filter where the emitter-follower was replaced by a single-phase multilevel half-bridge inverter, which is more suitable for voltage levels commonly used in frequency converters than the emitter-follower. In the simulations, the filter reduced all relevant quantities to about 2 % of the original values.

Modulation techniques have also been proposed for the reduction of the common-mode voltage of the inverter. Lai (1999) proposed a method that reduces the common-mode voltage by 50 %. It is based on a modulation pattern that does not apply zero vectors. Hence, the common-mode voltage will have only two possible values instead of four. This method is not suitable for modulation methods that actively use the zero vectors, such as the direct torque control (DTC). Manjrekar and Lipo (1999) proposed the zero vector to be produced by shorting the motor terminals with three auxiliary star-connected switches, which reduces the common-mode voltage without the restriction on the use of the zero vector. In a neutral point clamped (NPC) three-level inverter, it is possible to use only the voltage vectors that give exactly zero common-mode voltage (Ratnayake and Murai (1998)). However, such modulation reduces the number of applicable voltage vectors from the original 27 to 7.
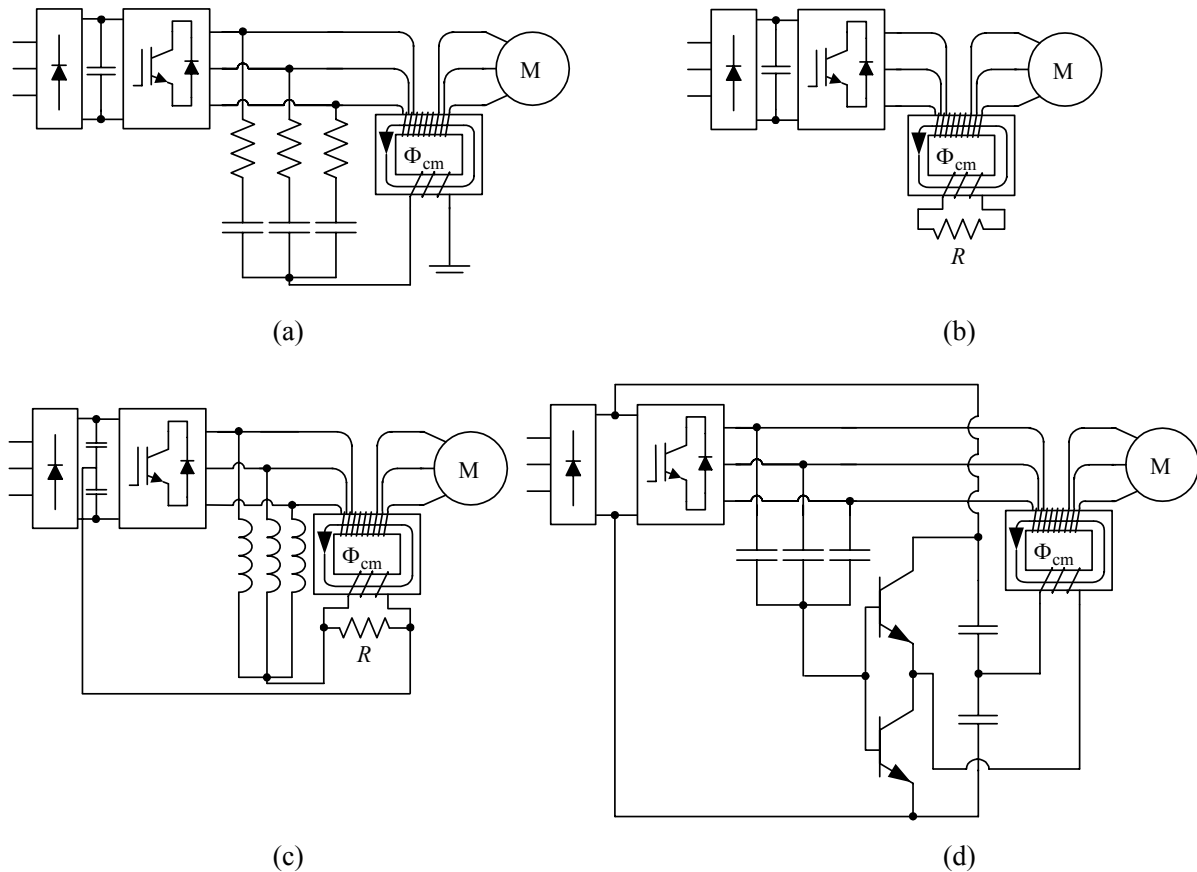
Fig 4.4. Common-mode voltage mitigation and cancellation schemes employing the common-mode transformer: (a) grounded secondary winding fed from artificial neutral point; (b) damping resistor connected to secondary winding; (c) neutral point formed by chokes, damping resistor, and connection to dc-link midpoint; (d) active compensator.

4.4 Special Converters

The converter topology can also be modified in such a way that the common-mode voltage is compensated. Several methods based on altering the number of inverter legs to an even number have been presented. The advantage of an even number of inverter legs is that the common-mode voltage, which is the average of the phase voltages, can be controlled to zero. Figure 4.5 illustrates the four-leg inverter suggested by Oriti et al. (1997b) and Julian et al. (1999). An auxiliary fourth leg is added to the inverter. The three primary legs are controlled normally, except that the zero vector (corresponding to three primary legs connected to the same dc bus) cannot be used, which somewhat restricts the useful modulation index. The fourth leg is controlled in such a way that two switches of the inverter are always connected to the positive dc bus and the other two to the negative dc bus. The common-mode voltage is thus zero. The current rating of the auxiliary fourth leg does not need to be as high as that of the other legs; in the experiment made by Julian et al. (1999), the fourth leg carried only 10 % of the current of the primary legs. Some passive components are also needed in the
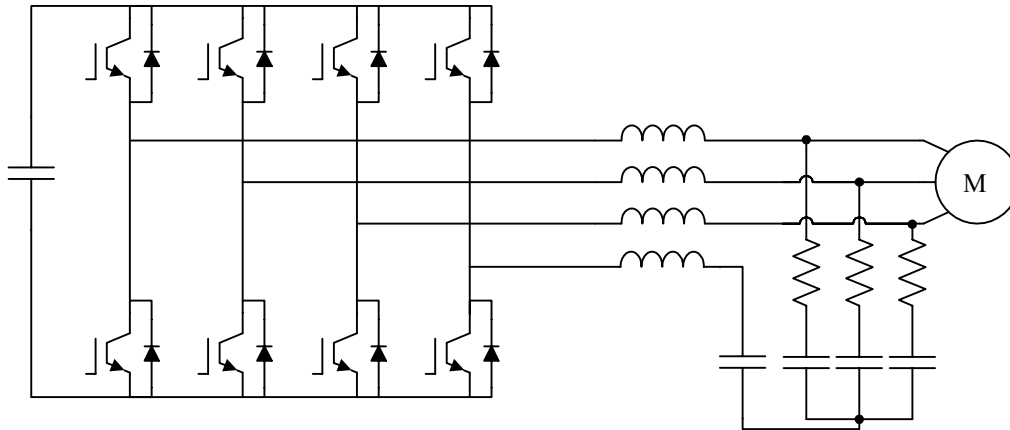
36

Fig 4.5. Four-leg inverter.

configuration. These components increase the risk of additional resonance frequencies in the system. Julian et al. (1999) also implemented the four-leg inverter in a resonant dc-link converter. The resonance frequency of the dc link was effectively attenuated at the inverter output.

The dual-bridge inverter (DBI) approach was presented by von Jouanne and Zhang (1999) for the cancellation of the common-mode voltage. The approach is based on feeding a suitably connected double-winding motor by two parallel inverters having opposite polarities, as illustrated in Fig. 4.6(a). The sum of these six phase voltages is always zero. In practice, any motor whose stator winding consists of an even number of parallel branches can be used. Re-connecting a two-branch winding for the DBI approach is illustrated in Figs. 4.6(b) and 4.6(c). Larger modifications may be needed if the branches are connected together inside the motor instead of the terminal box. The approach is applicable for both star and delta connected windings. The shaft voltage and the bearing current were virtually eliminated in a 5-hp drive used in the experiments (von Jouanne and Zhang 1999). The effectiveness of the DBI approach in the reduction of the conducted EMI was also demonstrated by Zhang and von Jouanne (1998)

In Publication VIII, the DBI approach was implemented in a 1.4-MW induction motor drive. In the experiments, a reduction of over 80 % is obtained in both the capacitive and induced shaft voltages. The remaining capacitive shaft voltage is found to originate from the common-mode voltage of the diode rectifier. This component of the common-mode voltage cannot be compensated by the DBI approach. The remaining induced shaft voltage is a result of a non-simultaneous timing of the PWM pulses of the parallel inverters. The significance of the time delay between the parallel inverters is investigated in Publication VIII using the simulation model presented in Publication VII. Simulations showed that a time delay as short as 15 ns between the parallel inverters is sufficient for causing the remaining induced shaft voltage in the investigated drive.

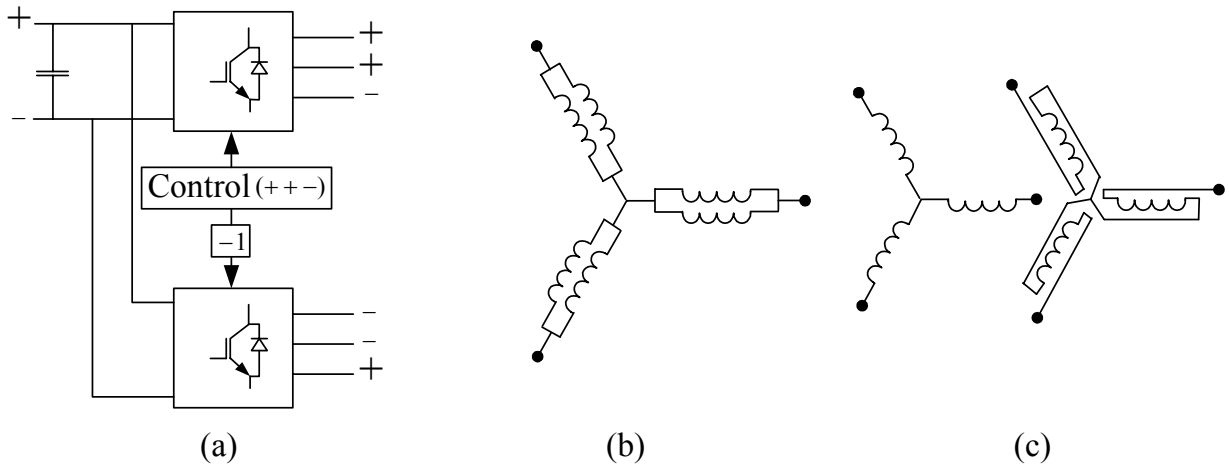(a)   (b)   (c)

Fig. 4.6. Dual bridge inverter approach: (a) dual-bridge inverter; (b) conventional two-branch winding; (c) winding prepared for DBI approach.

Oriti et al. (1997a) proposed a six-phase motor as a solution to the common-mode voltage problem. The stator winding of the motor consists of two three-phase windings at a 30-degree angle to each other. An even number of phases enables controlling the common-mode voltage to zero. In addition, an improved air-gap magnetomotive force is obtained with the winding, and the motor torque is smoother. Six legs are required in the inverter; the current rating of each inverter leg is half of the rating of a conventional three-phase inverter.

An open-end-winding motor fed by two two-level inverters was proposed by Baiju et al. (2004). The star point of the motor is opened, and two inverters having opposite polarities feed the ends of the winding. As in the DBI approach, the sum of the voltages is zero. Based on the observations of the DBI approach in Publication VIII, this method probably has the same restrictions as those of the DBI approach: the common-mode voltage originating from the rectifier is not compensated, and some induced shaft voltage will be present if the timing of the two inverters is not simultaneous. Moreover, an originally star-connected motor is needed for the open-end-winding connection.

4.5   *Discussion of the Mitigation Methods*

It is not easy to arrange the presented methods in any order according to their effectiveness or applicability. The methods that require substantial modifications to standard frequency converters (four-leg inverter), or require a special motor (shields, six-phase motor, open-end-winding motor) are probably less interesting for the manufacturers even if they were very effective for the bearing current reduction. Passive filters are relatively cheap, the availability of their components is good, and their installation is fast. Filters are also suitable for retrofitting. The drawback of all passive filtering methods is that they usually reduce only the high-frequency components of the common-mode current. Therefore, the capacitive shaft voltage is not reduced by these filters, unless the filter is made very large. Such filters are expensive, and may cause a substantial voltage drop in the differential-mode fundamental-

frequency voltage. The size of the drive has a significant effect on selecting a mitigation method for bearing currents. In large drives consisting of parallel inverter modules and cables, the DBI method can be implemented without any auxiliary components in some cases. Hybrid bearings are available for smaller motors, and also bearing insulations are more reliable in small motors because the mechanical stresses caused by the weight of the rotor are low. In severe cases, a combination of two methods may be required.

In practice, it is difficult to eliminate the shaft voltages and bearing currents altogether. Therefore, maximum values have been introduced for the shaft voltage. According to Erdman et al. (1996), shaft voltages below 0.3 V are safe and shaft voltages above 2 V may destroy the bearing. The maximum value for the shaft voltage is, however, difficult to generalize. Limits have also been suggested for the bearing current density, but there is no consensus about how high a bearing current density can be allowed. For example, according to Busse et al. (1997a), a bearing current density below 0.8 A/mm^2 does not reduce the mechanical life of bearings in PWM drives, whereas extensive tests made by Muetze et al. (2004) with four 11-kW motors suggest that bearing wear can be detected after just 50 h time of operation when the bearing current density is only 0.1 A/mm^2.

5   Experimental Setup

For the experiments presented in Publications V, VI, VII, and VIII, an experimental setup was built in the laboratory. The setup consists of two transformers, a frequency converter, motor cables, and a 1.4-MW cage induction motor. The ratings of the drive system components and the types of the measurement equipment are listed in Table 5.1.

The frequency converter was fed from a 400-V, 50-Hz distribution transformer via a 400 V/750 V autotransformer. The neutral point of the secondary winding of the distribution transformer was grounded. The frequency converter (1160 kVA, 690 V) has a single rectifier unit and two parallel inverter units. The dc-link voltage was 1013 V during the experiments. Four parallel 50 m long three-phase motor cables (MCMK 3x70/35) were used. The motor, the converter, and the transformer were placed on insulated foundations to break unwanted paths of the common-mode currents.

TABLE 5.1. TECHNICAL DATA OF THE LABORATORY HARDWARE

Induction motor	ABB HXR 500 LR6
	690 V, 75.4 Hz, 1500 r/min
	1.4 MW, 1410 A, $\cos\varphi = 0.85$
Frequency converter	ABB ACS 800 1160-7
Supply voltage	690 V
Nominal output current	970 A
Motor cable (four parallel cables)	Pirelli MCMK 3x70/35
Autotransformer	Trafotek 3PUK, 100kVA, 400/750 V
Supply transformer	500 kVA, 20.5 kV/410 V
	14.08 A/704.1 A Dyn 11
	$Z_k = 6.1$ %, $P_k = 6380$ W, $P_0 = 714$ W
Measuring equipment	
Common-mode current probe	Rogowski coil (Tampere University of Technology, 5MHz)
Shaft voltage probe	Tektronix P6139A, 10x, 500 MHz
Phase voltage probes	LeCroy PPE 2kV, 100x, 400 MHz
Oscilloscope	Tektronix TDS714L 500 MS/s
Impedance meter	Fluke PM6306 RCL-meter

The motor is a three-phase, six-pole cage induction motor (1.4 MW, 690 V, 1500 rpm, nominal frequency 75.4 Hz, shaft height 500 mm). Its stator winding is a two-layer form-wound winding with six parallel branches in delta connection. During the measurements, the motor was operating without load at 500 rpm. 10 mm thick bearing insulations and copper brush equipment at both shaft ends were installed in order to measure the voltage of the rotating shaft. An end shield with the insulation and the brush equipment is illustrated in Fig. 5.1.

The shaft voltage measurement is illustrated in Fig. 5.2. Both connections shown in the figure were open in the capacitive shaft voltage measurements, whereas the non-drive end of the shaft was shorted to the end-shield in the induced shaft voltage measurements. The phase voltages were measured with voltage probes connected between the phases and the motor frame. Three voltage probes were connected to form an artificial neutral point for measuring the common-mode voltage at the motor terminals, which enabled using only one channel of the oscilloscope for this measurement. The common-mode current of the motor was measured using a Rogowski coil around the phase conductors of the motor cables.

Fig. 5.1. End shield of the motor used in the experiments: insulation ring (A), copper brush (B), and slip ring (C).
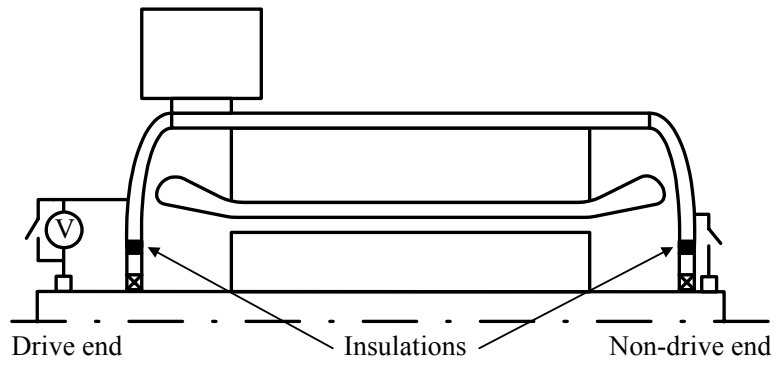
Fig. 5.2. The shaft voltage measurement setup in the experiments

6 Summaries of the Publications

The abstracts of the Publications are reprinted in Section 6.1. The common-mode flux distribution in the stator core is investigated in Publications I and II, whereas Publications III, IV, and VIII deal with methods for shaft voltage and bearing current mitigation. The focus in Publications V, VI, and VII is on the modeling the motor and other components of the electric drive system. The scientific contribution of the thesis is described in Section 6.2.

6.1 Abstracts

Publication I

A high-frequency common-mode current occurs in AC motors fed from frequency converters because of the very short rise time of inverter voltage pulses. The capacitive current causes electric and magnetic fields inside the stator iron core, possibly inducing a circulating-type bearing current. In the publication, the circumferential magnetic flux is investigated by means of finite element analysis and experiments. The high-frequency common-mode current generates a circumferential magnetic flux in the stator core. The experiment carried out without the rotor shows that a voltage is induced between the shaft ends by this circumferential flux. According to Ampère's law, the circumferential flux varies linearly in the axial direction in an ideal case. The finite-element analysis and the experiments also show the linear variation. Due to the high frequency of the common-mode current, the skin effect forces the current and the flux to flow at the surfaces of the iron sheets in the stator core. The common-mode current through the end windings and the biasing fundamental magnetic field also affect the circumferential flux and the voltage induced between the shaft ends.

Publication II

A high-frequency common-mode current appears in AC machines fed from frequency converters, causing a circumferential magnetic flux in the stator yoke. This flux induces a voltage between the shaft ends and can cause circulating-type bearing currents. The finite element solution of the field problem shows that the common-mode impedance of the core region depends only on the capacitance of the winding insulation in a wide frequency range, whereas the circumferential magnetic flux and the shaft voltage are strongly dependent on the skin depth in the stator laminations.

Publication III

The paper analyses a shielding method against circulating-type bearing currents in converter-fed AC machines. These currents are induced by the high-frequency flux components that are generated by the common-mode current penetrating the stator core. A conductive shield is placed in the stator slots between the winding and the core, providing a low-impedance path for high-frequency common-mode currents. The shielding effectiveness is analysed using a circuit model, and the fundamental-frequency losses in the shield are analysed by a two-dimensional finite element method and an analytical formulation. The analysis shows that the current penetrating the stator core is attenuated very effectively. The losses in the shield can be reduced to an acceptable level by proper shield thickness selection or by splitting the shield into axial strips.

Publication IV

New design principles are proposed for reducing the bearing currents in converter-fed induction motors. Simple qualitative analysis is used for the investigation. According to the analysis presented in the paper, the shaft potential and the induced shaft voltage can be reduced by motor design. In this respect, the most significant parameters are the diameter-to-length ratio of the core and the number of poles of the motor.

Publication V

The paper presents a method for the modeling of three-phase power cables in circuit simulation software, applicable to the analysis of ac motor drives where steep voltage pulses are produced by frequency converters. Both differential-mode and common-mode phenomena are considered. The cable is represented by a number of lumped-parameter segments, including ladder networks for taking the frequency-dependence of the parameters into account. Methods studied for the evaluation of the model parameters are the finite element method, approximate analytical expressions, and measurements. The accuracy of the model is demonstrated by comparing simulation results with measurement results. The model is suitable for transient and harmonic analyses in a wide frequency band.

Publication VI

The paper proposes a three-phase motor model that is suitable for the analysis of bearing voltages and currents in converter-fed ac motors. Both capacitive and induced shaft voltages are taken into account. The induced shaft voltage, being the reason for high-frequency circulating bearing currents, is important in larger machines. For modeling the induced shaft voltage with a sufficient accuracy, different stator core models are compared. The motor model can be connected to three-phase circuit simulation models of frequency converters and cables. Simulation results are validated with experimental results obtained using a 1.4-MW induction motor fed by a frequency converter.

Publication VII

The paper presents a circuit simulation model for ac drive systems, including the capacitive and induced shaft voltages that are caused by frequency converters in ac motors. For bearing current analysis, it is essential that the common-mode voltages and currents can be predicted with a sufficient accuracy in an adequate bandwidth. The system model consists of three-phase circuit models for the power supply, the frequency converter, the motor cable, and the induction motor. The simulation results are compared with experimental results from a 1.4-MW induction motor drive. Good accuracy is achieved in predicting common-mode voltages, common-mode currents, and induced shaft voltages.

Publication VIII

The dual-bridge inverter (DBI) approach, developed to eliminate the common-mode voltage and resulting bearing current generated by frequency converters, is investigated by means of experiments and simulations. The approach reduces the capacitive and induced shaft voltages by more than 80 % in the examined 1.4 MW induction motor drive. The remaining shaft voltage is found to be caused by the rectifier-generated common-mode voltage and a time delay between the PWM pulses of the parallel inverter units.

6.2   Contribution of the Thesis

The main scientific contributions in the Publications of this thesis are:

- The axial distribution of the high-frequency circumferential magnetic flux is measured in Publication I. The explanation given for this distribution is the basis for the development of induced shaft voltage models.

- A numerical model is developed for the high-frequency electromagnetic field in the stator core and winding insulation in Publication II. It is shown that the common-mode current penetrating the stator core is responsible of the circumferential flux. Analytical expressions are derived for the circumferential flux and the common-mode impedance of the stator core.

- A conductive shield placed in the stator slots is analyzed in Publication III exploiting the analytical expressions derived in Publication II. The shield was originally proposed by Schüren (2001) for mitigating the common-mode current in the core. The selection of the shield thickness and the subdivision of the shield into strips are also investigated.

- New design principles are proposed in Publication IV for converter-fed ac motors. With respect to the shaft voltages, it is advisable to have a high number of poles and a large diameter-to-length ratio of the core.

- The evaluation of the parameters for the motor cable model originally presented by Tellinen (1999) is clarified in Publication V. Regardless of different magnetic field distributions for the common and differential modes, the parameters of the model can be evaluated for the common mode without compromising the differential-mode accuracy.

- A novel circuit model for the analysis of capacitive and induced shaft voltages is presented in Publication VI based on the results of Publication II. The resulting three-phase induction motor model can be connected to the models of other drive system components.

- A three-phase model for the whole drive system is implemented in circuit simulation software in Publication VII, and used for the analysis of common-mode phenomena and shaft voltages. The publication demonstrates the importance of the common-mode impedance distribution in the drive system when shaft voltages are analyzed.

- In Publication VIII, the dual-bridge inverter approach, proposed originally by von Jouanne and Zhang (1999), is implemented in a 1.4-MW induction motor drive. The restrictions of the method are investigated by means of experiments and simulations, and the reasons for the remaining capacitive and induced shaft voltages are explained.

7   Conclusion

The bearing currents generated by frequency converters originate from a nonzero common-mode voltage at the motor terminals. The parasitic capacitances of the motor cause a shaft voltage with respect to the ground. This voltage follows the waveform of the common-mode voltage. High-frequency components of the common-mode current in the stator core cause a circumferential magnetic flux, which induces a voltage between the shaft ends.

In the thesis, the circumferential magnetic flux is analyzed by means of experiments and numerical models, and analytical expressions are derived for the flux. A circuit model of the induced shaft voltage phenomenon is presented. This model is combined with a model of the capacitive shaft voltage and a three-phase model of the induction motor. The model is validated by comparing simulation and experimental results.

In addition to the motor, the contributions of other drive system components to the common-mode impedance are shown to be important in the modeling of the shaft voltage phenomena. In order to get a correct common-mode voltage at the motor terminals, the motor model is included in a complete model of the electric drive system, consisting of the models of the power grid, the frequency converter, and the motor cables. Good correlation is found between the simulation and experimental results.

The derived expressions and the simulation model are used for investigating mitigation methods for the induced shaft voltage. A conductive shield in stator slots, originally proposed by Schüren (2001), is investigated by using a simple common-mode model, and shown to have potential for the mitigation of the induced shaft voltage. The dual-bridge inverter approach (DBI), proposed by von Jouanne and Zhang (1999), is investigated experimentally and by simulations with a 1.4-MW induction motor drive. The DBI approach is shown to be a promising method for the mitigation of both capacitive and induced shaft voltages if the imperfections of the method presented in Publication VIII are acceptable or can be removed.

It is also shown that modifications in the motor design can reduce the induced shaft voltage. Hence, new design principles are proposed for converter-fed induction motors.

A suitable topic for future research is to apply the presented motor model to other cases, e.g., different motor sizes and designs, and higher levels of magnetic saturation. In this way, additional information could be gained about the selection of the incremental permeability value to be used and about the assumption of constant common-mode voltage in the stator winding.

Bibliography

Ahola, J., Lindh, T. and Partanen, J. (2003), "Simulation model for input impedance of low voltage electric motor at frequency band 10 kHz - 30 MHz," in *Proceedings of the IEEE International Electric Machines and Drives Conference*, *IEMDC'03*, Madison, WI, pp. 1127-1132.

Akagi, H. and Doumoto, T. (2004), "An approach to eliminating high-frequency shaft voltage and leakage current from an inverter-driven motor," *IEEE Transactions on Industry Applications,* **40,** pp. 1162-1169.

Ammann, C., Reichert, K., Joho, R. and Posedel, Z. (1988), "Shaft voltages in generators with static exitation systems - problems and solution," *IEEE Transactions on Energy Conversion,* **3,** pp. 409-419.

Baiju, M. R., Mohapatra, K. K., Kanchan, R. S. and Gopakumar, K. (2004), "A dual two-level inverter scheme with common mode voltage elimination for an induction motor," *IEEE Transactions on Power Electronics,* **19,** pp. 794-805.

Barker, S. (2000), "Avoiding premature bearing failure with inverter fed induction motors," *IEEE Power Engineering Journal,* **14,** pp. 182-189.

Boglietti, A. and Carpaneto, E. (1999), "Induction motor high frequency model," in *Conference Record of the 34th IEEE-IAS Annual Meeting*, *IAS'99*, Phoenix, AZ, vol. 3, pp. 1551-1558.

Boglietti, A. and Carpaneto, E. (2001), "An accurate induction motor high-frequency model for electromagnetic compatibility analysis," *Electric Power Components and Systems,* **29,** pp. 191-209.

Bozorth, R. M. (1993) *Ferromagnetism,* IEEE Press, New York.

Busse, D., Erdman, J. M., Kerkman, R. J., Schlegel, D. W. and Skibinski, G. L. (1997a), "Bearing currents and their relationship to PWM drives," *IEEE Transactions on Power Electronics,* **12,** pp. 243-251.

Busse, D., Erdman, J. M., Kerkman, R. J., Schlegel, D. W. and Skibinski, G. L. (1997b), "The effects of PWM voltage source inverters on the mechanical performance of rolling bearings," *IEEE Transactions on Industry Applications,* **33,** pp. 567-575.

Busse, D., Erdman, J. M., Kerkman, R. J., Schlegel, D. W. and Skibinski, G. L. (1997c), "An evaluation of the electrostatic shielded induction motor: a solution for rotor shaft voltage buildup and bearing current," *IEEE Transactions on Industry Applications,* **33,** pp. 1563-1570.

Busse, D., Erdman, J. M., Kerkman, R. J., Schlegel, D. W. and Skibinski, G. L. (1997d), "System electrical parameters and their effects on bearing currents," *IEEE Transactions on Industry Applications,* **33,** pp. 577-584.

Cacciato, M. and Testa, A. (2000), "High frequency modeling of induction motors," in *Proceedings of Symposium on Power Electronics, Electrical Drives, Automation & Motion, SPEEDAM'00*, Ischia, Italy, vol. C2, pp. 13-18.

Chen, S., Lipo, T. A. and Fitzgerald, D. (1995), "Measurement and analysis of induction motor bearing currents in in PWM inverter drives," in *Proceedings of the International Aegean Conference on Electrical Machines and Power Electronics*, Kusadasi, Turkey, pp. 289-296.

Chen, S., Lipo, T. A. and Fitzgerald, D. (1996a), "Modeling of motor bearing currents in PWM inverter drives," *IEEE Transactions on Industry Applications,* **32,** pp. 1365-1370.

Chen, S., Lipo, T. A. and Fitzgerald, D. (1996b), "Source of induction motor bearing currents caused by PWM inverters," *IEEE Transactions on Energy Conversion,* **11,** pp. 25-32.

Chen, S., Lipo, T. A. and Novotny, D. W. (1996c), "Circulating type motor bearing current in inverter drives," in *Conference Record of the 31st IEEE-IAS Annual Meeting, IAS'96*, San Diego, CA, vol. 1, pp. 162-167.

Consoli, A., Oriti, G. and Testa, A. (1996), "Induction motor modeling for common mode and differential mode emission evaluation," in *Conference Record of the 31st IEEE-IAS Annual Meeting, IAS'96*, San Diego, CA, vol. 1, pp. 595-599.

Costello, M. J. (1993), "Shaft voltages and rotating machinery," *IEEE Transactions on Industry Applications,* 29, pp. 419-426.

Dolezel, I., Valouch, V. and Skramlik, J. (2000), "High frequency models of transistor voltage inverter-fed induction motor drives," in *Proceedings of IEEE International Conference on Industrial Technology, ICIT'00*, Goa, India, vol. 2, pp. 32-37.

Erdman, J. M., Kerkman, R. J., Schlegel, D. W. and Skibinski, G. L. (1996), "Effect of PWM inverters on AC motor bearing currents and shaft voltages," *IEEE Transactions on Industry Applications,* **32,** pp. 250-259.

Fleischmann, L. (1909), "Ströme in Lagern und Wellen," *Elektrische Kraftbetriebe und Bahnen,* **7,** pp. 352-353.

Fröberg, V. (2003), "Du/dt- and bearing current filtering for frequency converter drives", Master's thesis, Espoo, Finland, Helsinki University of Technology, Department of Electrical and Communications Engineering, 102 p.

Grandi, G., Casadei, D. and Massarini, A. (1997), "High frequency lumped parameter model for AC motor windings," in *Proceedings of the 7th European Conference on Power Electronics and Applications*, *EPE'97*, Trondheim, Norway, vol. 2, pp. 578-583.

Habetler, T., Naik, R. and Nondahl, T. (2002), "Design and implementation of an inverter output LC filter used for dv/dt reduction," *IEEE Transactions on Power Electronics,* **17,** pp. 327-331.

Hanigovszki, N., Poulsen, J. and Blaabjerg, F. (2004), "A novel output filter topology to reduce motor overvoltage," *IEEE Transactions on Industry Applications,* **40,** pp. 845-852.

Hausberg, V. and Seinch, H. (2000a), "Kapazitive Lagerspannungen und -ströme bei umrichtergespeisten Induktionsmaschinen," *Electrical Engineering,* **82,** pp. 153-162.

Hausberg, V. and Seinch, H. (2000b), "Wellenspannungen und zirkulierende Lagerströme bei Umrichtergespeisten Induktionsmaschinen," *Electrical Engineering,* **82,** pp. 313-326.

Hofmann, L. (2003), "Cable model with frequency dependent parameters calculated by using subconductors," *European Transactions on Electrical Power,* **13,** pp. 15-22.

Hussein, A. and Joos, G. (1997), "Modeling and simulation of traveling waves in induction motor drives," in *Proceedings the 12th of Applied Power Electronics Conference and Exposition*, *APEC'97*, Atlanta, GA, vol. 1, pp. 128-134.

Hyypio, D. (2005), "Mitigation of bearing electro-erosion of inverter-fed motors through passive common-mode voltage suppresion," *IEEE Transactions on Industry Applications,* **41,** pp. 576-583.

Julian, A. L., Oriti, G. and Lipo, T. A. (1999), "Elimination of common-mode voltage in three-phase sinusoidal power converters," *IEEE Transactions on Power Electronics,* **14,** pp. 982- 989.

Kerszenbaum, I. (1992), "Shaft currents in electric machines fed by solid-state drives," in *Conference Record of the Industrial and Commercial Power Systems Technical Conference*, Pittsburgh, PA, pp. 71-79.

Kim, J.-S. and Nam, K.-H. (2000), "A method of lowering bearing current with embedded circular comb-like coil," in *Conference Record of the 35th IEEE-IAS Annual Meeting*, *IAS'00*, Rome, Italy, vol. 3, pp. 1670-1674.

Kim, S. and Neikirk, D. P. (1996), "Compact equivalent circuit model for the skin effect," *IEEE-MMT-S International Microwave Symposium*, San Francisco, CA, vol. 3, pp. 1815-1818.

Lai, Y. S. (1999), "New random technique of inverter control for common mode voltage reduction of inverter-fed induction motor drives," *IEEE Transactions on Energy Conversion,* **14,** pp. 1139-1146.

Link, P. J. (1999), "Minimizing electric bearing currents in ASD systems," *IEEE Industry Applications Magazine,* **5,** pp. 55-66.

Manjrekar, M. and Lipo, T. A. (1999), "An auxiliary zero state synthesizer to reduce common mode voltage in three-phase inverters," in *Conference Record of the 34th IEEE-IAS Annual Meeting, IAS'99*, Phoenix, AZ, vol. 1, pp. 54-59.

Moreira, A. F., Lipo, T. A., Venkataramanan, G. and Bernet, S. (2001), "High frequency modeling for cable and induction motor overvoltage studies in long cable drives," *IEEE Transactions on Industry Applications,* **38,** pp. 1297-1306.

Moreira, A. F., Santos, P. M., Lipo, T. A. and Venkataramanan, G. (2005), "Filter networks for long cable drives and their influence on motor voltage distribution and common-mode current," *IEEE Transactions on Industial Electronics,* **52,** pp. 515-522.

Muetze, A. and Binder, A. (2002), "Influence of motor size on the nature of bearing currents - investigations at 11kW and 110 kW inverter-fed induction motors," in *Proceedings of the International Conference on Power Electronics, Intelligent Motion, and Power Quality, PCIM '02*, Nürnberg, Germany.

Muetze, A., Binder, A., Vogel, H. and Hering, J. (2004), "Experimental evaluation of the endangerment of ball bearings due to inverter-induced bearing currents," in *Conference Record of the 39th IEEE-IAS Annual Meeting, IAS'04*, Seattle, WA, vol. 3., pp. 1989-1995.

Muetze, A., De Gersem, H. and Weiland, T. (2005), "Influence of teeth and cooling ducts on the high-frequency common mode flux of inverter-fed ac machines", in *Conference Record of the 40th IEEE-IAS Annual Meeting, IAS'05*, Hong Kong, vol. 2, pp. 1350-1356.

Murai, Y., Kubota, T. and Yoshihiro, K. (1992), "Leakage current reduction for a high-frequency carrier inverter feeding an induction motor," *IEEE Transactions on Industry Applications,* **28,** pp. 858-863.

Naik, R., Nondahl, T., Melfi, M., Schiferl, R. and Wang, J. (2003), "Circuit model for shaft voltage prediction in induction motors fed by PWM-based AC drives," *IEEE Transactions on Industry Applications,* **39,** pp. 1294-1299.

Ogasawara, S. and Akagi, H. (1996), "Modeling and damping of high-frequency leakage currents in PWM inverter-fed AC motor drive systems," *IEEE Transactions on Industry Applications,* **32,** pp. 1105-1114.

Ogasawara, S. and Hideki, A. (1998), "An active circuit for cancellation of common-mode voltage generated by a PWM inverter," *IEEE Transactions on Power Electronics,* **13,** pp. 835-841.

Ollila, J., Hammar, T., Iisakkala, J. and Tuusa, H. (1997a), "A new reason for bearing current damages in variable speed drives," in *Proceedings of th European Conference on Power Electronics and Applications*, *EPE'97*, Trondheim, Norway, vol. 2, pp. 539-542.

Ollila, J., Hammar, T., Iisakkala, J. and Tuusa, H. (1997b), "On the bearing currents in medium power variable speed AC drives," in *Proceedings of the International Electric Machines and Drives Conference*, *IEMDC'97*, Milwaukee, WI, pp. MD1/1.1-MD1/1.3.

Oriti, G., Julian, A. L. and Lipo, T. A. (1997a), "An inverter/motor drive with common mode voltage elimination," in *Conference Record of the 32nd IEEE-IAS Annual Meeting*, *IAS'97*, New Orleans, LA, vol. 1, pp. 587-592.

Oriti, G., Julian, A. L. and Lipo, T. A. (1997b), "A new space vector modulation strategy for common mode voltage reduction," in *Conference Record of the 28th IEEE Power Electronics Specialists Conference*, *PESC'97*, St. Louis, MO, vol. 2, pp. 1541-1546.

Palma, L. and Enjeti, P. (2002), "An inverter output filter to mitigate dv/dt effects in PWM drive systems," in *Proceedings the 17th of Applied Power Electronics Conference and Exposition*, *APEC'02*, Dallas, TX, vol. 1, pp. 550-556.

Pillay, P. and Levin, V. (1995), "Mathematical models for induction machines," in *Conference Record of the 30th IEEE-IAS Annual Meeting*, *IAS'95*, Orlando, FL, vol. 1, pp. 606-616.

Punga, F. and Hess, W. (1907), "Eine Erscheinung an Wechsel- und Drehstromgeneratoren," *Elektrotechnik und Maschinenbau,* **25,** pp. 615-618.

Ramo, S., Whinnery, J. R. and Van Duzer, T. (1965) *Fields and Waves in Communication Electronics,* John Wiley and Sons, Inc., New York.

Ratnayake, K. R. M. N. and Murai, Y. (1998), "A novel PWM scheme to eliminate common-mode voltage in three-level voltage source inverter," in *Conference Record of 29th IEEE Power Electronics Specialists Conference*, *PESC'98*, Fukuoka, Japan, vol. 1, pp. 269-274.

Rendusara, D. and Enjeti, P. (1998a), "An improved inverter output filter configuration reduces common and differential modes dv/dt at the motor terminals in PWM drive systems," *IEEE Transactions on Power Electronics,* **13,** pp. 1135-1143.

Rendusara, D. and Enjeti, P. (1998b), "A method to reduce common mode & differential mode dv/dt at the motor terminals in PWM rectifier/PWM inverter type adjustable speed drive systems," in *Proceedings the 13th of Applied Power Electronics Conference and Exposition*, *APEC'98*, Anaheim, CA, vol. 2, pp. 1010 -1016.

Schlegel, D. W., Wrate, G., Kerkman, R. J. and Skibinski, G. L. (1999), "Resonant tank motor model for voltage reflection simulations with PWM drives," in *Proceedings of the IEEE Electric Machines and Drives Conference*, *IEMDC'99*, Seattle, WA, pp. 463-465.

Schüren, V. (2001) German Patent 199 48 145 C 1.

Sheng, K., Williams, B. and Finney, S. (2000), "A review of IGBT models," *IEEE Transactions on Power Electronics,* **15,** pp. 1250-1266.

Skibinski, G. L., Kerkman, R. J., Leggate, D., Pankau, J. and Schlegel, D. W. (1998), "Reflected wave modeling techniques for PWM AC motor drives," in *Proceedings of the 13th Applied Power Electronics Conference and Exposition*, *APEC'98*, Anaheim, CA, vol. 2, pp. 1021-1029.

Suralac ® Coatings, Surahammars Bruk, www.sura.se

Swamy, M., Yamada, K. and Kume, T. (2001), "Common mode current attenuation techniques for use with PWM drives," *IEEE Transactions on Power Electronics,* **16,** pp. 248-255.

Tellinen, J. (1999) *EMC Modeling of Magnetic Components,* Report 57, Helsinki University of Technology, Laboratory of Electromechanics (in Finnish).

von Jouanne, A. and Enjeti, P. (1997), "Design considerations for an inverter output filter to mitigate the effects of long motor leads in ASD applications," *IEEE Transactions on Industry Applications,* **33,** pp. 1138-1145.

von Jouanne, A., Enjeti, P. and Gray, W. (1995), "The effect of long motor leads on pwm inverter fed ac motor drive system," in *Proceedings the 10th of Applied Power Electronics Conference and Exposition*, *APEC'95*, Dallas, TX, vol. 2, pp. 592- 597.

von Jouanne, A., Rendusara, D., Enjeti, P. and Gray, W. (1996), "Filtering techniques to minimize the effect of long motor leads on PWM inverter-fed AC motor drive systems," *IEEE Transactions on Industry Applications,* **32,** pp. 919-926.

von Jouanne, A. and Zhang, H. (1999), "A dual-bridge inverter approach to eliminating common-mode voltages and bearing and leakage currents," *IEEE Transactions on Power Electronics,* **14,** pp. 43-48.

Xiang, Y. Q. (1998), "A novel active common-mode-voltage compensator (ACCom) for bearing current reduction of PWM VSI-fed induction motors," in *Proceedings of the 13th*

Applied Power Electronics Conference and Exposition, *APEC '98*, Anaheim, CA, vol. 2, pp. 1003-1009.

Yen, C.-S., Fazarinc, Z. and Wheeler, R. L. (1982), "Time-domain skin-effect model for transient analysis of lossy transmission lines," *Proceedings of the IEEE,* **70,** pp. 750-757.

Zhang, H. and von Jouanne, A. (1998), "Suppressing common-mode conducted EMI generated by PWM drive systems using a dual-bridge inverter," in *Proceedings of the 13th Applied Power Electronics Conference and Exposition*, *APEC '98*, Anaheim, CA, vol. 2, pp. 1017- 1020.

Appendix I

Core Impedance and Circumferential Flux

In Publication II, the expressions for the circumferential magnetic flux in the stator yoke and the common-mode impedance of the stator core are presented. These expressions are derived in the following. The problem is simplified by assuming that in the stator core, the common-mode current and the corresponding magnetic field flow only in the yoke and the frame, as illustrated in Fig. 3.3. The magnetic flux in each lamination can be considered as a sum of two flux components: the flux generated by the current flowing into the lamination in question through the stator winding insulation and the flux generated by the current flowing from the adjacent lamination, as demonstrated in Publication II.

If an equal current is assumed to flow into each lamination through the winding insulation (i.e. the capacitance of the winding insulation dominates in the common-mode impedance), the flux of each lamination can be calculated based on the flux of a single lamination. The expression of the magnetic flux corresponding to the case of the rightmost lamination in Fig. 3.3 is derived in the following, and the flux of this lamination is used for the derivation of the total common-mode flux of the core. The material properties are assumed constant in the analysis. In the frequency band relevant to the problem, the skin depth is much smaller than the thickness of a lamination. Thus the electromagnetic field at each lamination surface can be modeled as a field of a plane conductor of infinite depth.

The azimuthal magnetic field strength in a plane conductor of infinite depth (Ramo et al. 1965) in cylindral r-φ-z coordinates is

$$\underline{H}_\varphi = \underline{H}_0 e^{-\frac{1+j}{\delta}z} \tag{A.1}$$

where $\underline{H}_0$ is the magnetic field strength at the surface of the conductor and δ is the skin depth defined as

$$\delta = \sqrt{\frac{2}{\omega\mu\sigma}} \tag{A.2}$$

where ω is the angular frequency, σ the conductivity, and μ the incremental permeability. The examined geometry is depicted in Fig. A1.1. The magnetic field strength at the lamination surface has a radial variation:
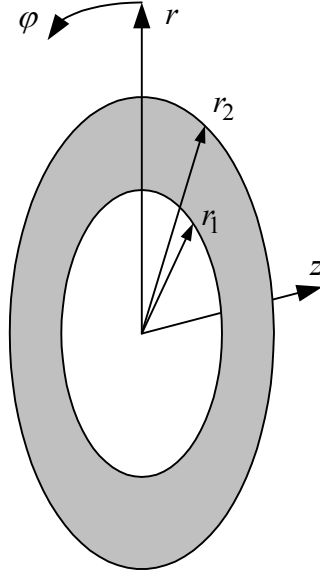
Fig. A1.1. The geometry, denotations and coordinates used in the derivations.

$$\underline{H}_0 = \frac{\underline{i}_1}{2\pi r} \tag{A.3}$$

where $\underline{i}_1$ is the current flowing in the neighborhood of the lamination surface in the radial direction.

The magnetic flux in a single lamination is obtained as a surface integral over the cross-section of the lamination,

$$
\begin{aligned}
\underline{\phi}_1 &= \int_A \mu \underline{H}_\varphi \, \mathrm{d}A \\
&= \int_0^\infty \int_{r_1}^{r_2} \mu \frac{\underline{i}_1}{2\pi r} e^{-\frac{1+\mathrm{j}}{\delta} z} \, \mathrm{d}r \, \mathrm{d}z \\
&= \frac{\mu \delta \underline{i}_1}{2\pi(1+\mathrm{j})} \ln\left(\frac{r_2}{r_1}\right)
\end{aligned}
\tag{A.4}
$$

where r_1 and r_2 are the inner and outer radii of the stator yoke, respectively. The common-mode flux of the stator core is derived assuming that equal currents flow into each of the N laminations through the winding insulation. The common-mode current is $\underline{i}_{cm}$, and the current

$$\underline{i}_1 = \frac{\underline{i}_{cm}}{N} \tag{A.5}$$

flows into each lamination. It causes the flux contribution $\underline{\phi}_1$ to this lamination and $2\underline{\phi}_1$ to all laminations to the left, in accordance with Fig. 3.3. The total common-mode flux is the sum of the fluxes in all laminations:

$$
\begin{aligned}
\underline{\phi}_{cm} &= \underline{\phi}_1 + \underline{\phi}_2 + \underline{\phi}_3 + \ldots + \underline{\phi}_N \\
&= \underline{\phi}_1 \left(1 + 3 + 5 + \ldots + 2N - 1\right) \\
&= N^2 \underline{\phi}_1.
\end{aligned}
\tag{A.6}
$$

Substitution of (A.4) and (A.5) in (A.6) gives

$$
\underline{\phi}_{cm} = \frac{\mu\delta N \underline{i}_{cm}}{2\pi(1+j)} \ln\left(\frac{r_2}{r_1}\right).
\tag{A.7}
$$

The common-mode impedance of the stator core is derived assuming again that equal currents flow into each lamination through the winding insulation. The resistance of one side of the lamination is

$$
R_1 = \frac{1}{2\pi\sigma\delta} \ln\left(\frac{r_2}{r_1}\right)
\tag{A.8}
$$

and the resistive losses in the lamination are

$$
P_1 = R_1 i_1^2.
\tag{A.9}
$$

The total resistive losses in the core are obtained as a sum of the losses at each lamination surface,

$$
\begin{aligned}
P_{tot} &= 2R_1 i_1^2 + 2R_1 (2i_1)^2 + \ldots + 2R_1\left[(N-1)i_1\right]^2 + R_1(Ni_1)^2 \\
&= 2R_1 i_1^2 \left[1 + 2^2 + \ldots + (N-1)^2 + \frac{1}{2}N^2\right] \\
&\approx 2R_1 i_1^2 \left(\frac{N^3}{3} + \frac{N^2}{2} + \frac{N}{6}\right) \\
&\approx 2R_1 i_1^2 \frac{N^3}{3}
\end{aligned}
\tag{A.10}
$$

where the two last forms hold for large N. Substituting (A.8) and (A.5) in (A.10) yields

$$
P_{tot} = \frac{N}{3\pi\sigma\delta} \ln\left(\frac{r_2}{r_1}\right) i_{cm}^2
\tag{A.11}
$$

Thus the common-mode resistance of the core is

$$R_c = \frac{N}{3\pi\sigma\delta} \ln\left(\frac{r_2}{r_1}\right). \tag{A.12}$$

Regardless of the frequency, the reactance of a plane conductor of infinite depth is equal to the resistance (Ramo et al. 1965). Therefore, the inductance is simply

$$L_c = \frac{R_c}{\omega}. \tag{A.13}$$

A combination of (A.12) and (A.13) gives the common-mode impedance of the stator core:

$$\underline{Z}_c = (1+j)\frac{N}{3\pi\sigma\delta} \ln\left(\frac{r_2}{r_1}\right). \tag{A.14}$$

The stator core also has a contribution to the bearing circuit impedance. The circulating bearing current flows along each lamination causing an equal magnetic flux in each sheet. Therefore, the stator core impedance for the bearing circuit is simply

$$\underline{Z}_d = 3\underline{Z}_c. \tag{A.15}$$

Appendix II

Effects of Lamination Insulation

In principle, the insulation between the laminations of the stator core has an effect on the common-mode impedance because the resistance and the capacitance of the insulation provide an alternative path for the common-mode current to flow. The significance of this effect is investigated here by calculating the impedance between the ends of two adjacent laminations and the magnetic flux in these laminations. Three different models, depicted in Fig. A2.1, are compared: the impedance in the case of infinite insulation impedance ($\underline{Z}_A$); a T-equivalent circuit with the lamination insulation modeled by a resistance and a capacitance ($\underline{Z}_B$); and a 10-ladder circuit ($\underline{Z}_C$). The resistance and the thickness of the insulation are taken from the website of the lamination manufacturer (Surahammars Bruk). They are listed in Table A.I. The permittivity of the insulation material is not given by the manufacturer, the relative permittivity used in the analysis is 4.
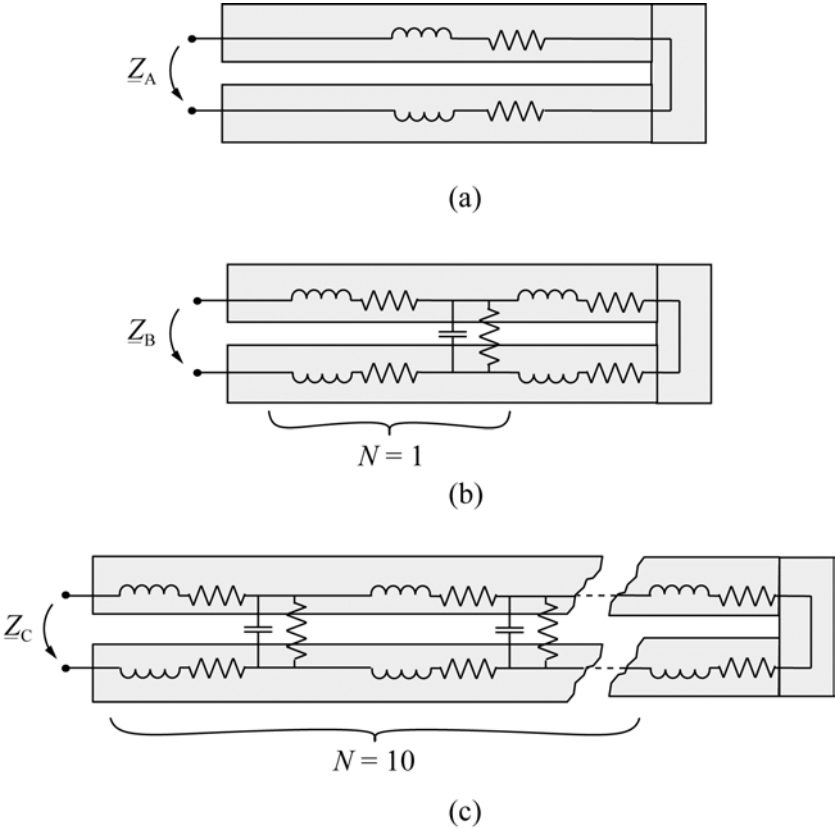

(a)

(b)

$N = 1$

(c)

$N = 10$

Fig. A2.1. Iron lamination impedance models used in the analysis: (a) infinite insulation impedance, (b) a T-equivalent circuit with the lamination insulation modeled by a resistance and a capacitance, and (c) a 10-ladder circuit.

	Suralac 3000	Suralac 5000
Thickness (μm)	3.5–6	0.7–1.2
Standard thickness (μm)	6	1.2
Surface insulation resistance Ωcm^2 (min. thickness)	>200	5
Surface insulation resistance Ωcm^2 (standard thickness)	>200	20

In practice, the manufacturing process of the core leaves gaps much larger between the laminations than the insulation thicknesses indicate (the minimum thickness of Suralac 5000 insulation would lead to an overly optimistic fill factor of 99.7 % in the core). These gaps are consequently filled with insulation in the vacuum impregnation process. Therefore, the presented analysis can be considered as a worst case. The minimum values of the thickness and surface resistance are used in the analysis. The values of Table A.I are given for one side of the lamination. They are multiplied by two for the analysis.

The magnitude and phase of the impedances $\underline{Z}_A$, $\underline{Z}_B$ and $\underline{Z}_C$ are shown in Fig. A2.2 for Suralac 3000 coating. Increasing the number of subcircuits from one in the simple T-equivalent circuit to a 10-ladder circuit has only a small effect on the impedance in the investigated frequency band. The difference to the model with infinite insulation impedance is visible only in the phase curves at very high frequencies. The magnetic flux in the laminations is shown relative to the case of infinite insulation impedance in Fig. A2.3. The models give equal fluxes below 1 MHz. At 10 MHz the magnetic flux has increased less than 5 percent.

The analysis is repeated for Suralac 5000 coating. The impedances of the three models are shown in Fig. A2.4. The difference is again visible only in the phase curve. The magnetic flux relative to the case without the insulation model is shown in Fig. A2.5. Because of a much smaller surface resistance of the insulation, the effect of the insulation is more pronounced than in the case of Suralac 3000 insulation.

The results indicate that even in the worst case, the insulation impedance has only a minor effect on the core impedance and the circumferential magnetic flux. Therefore, it can be ignored in the modeling.
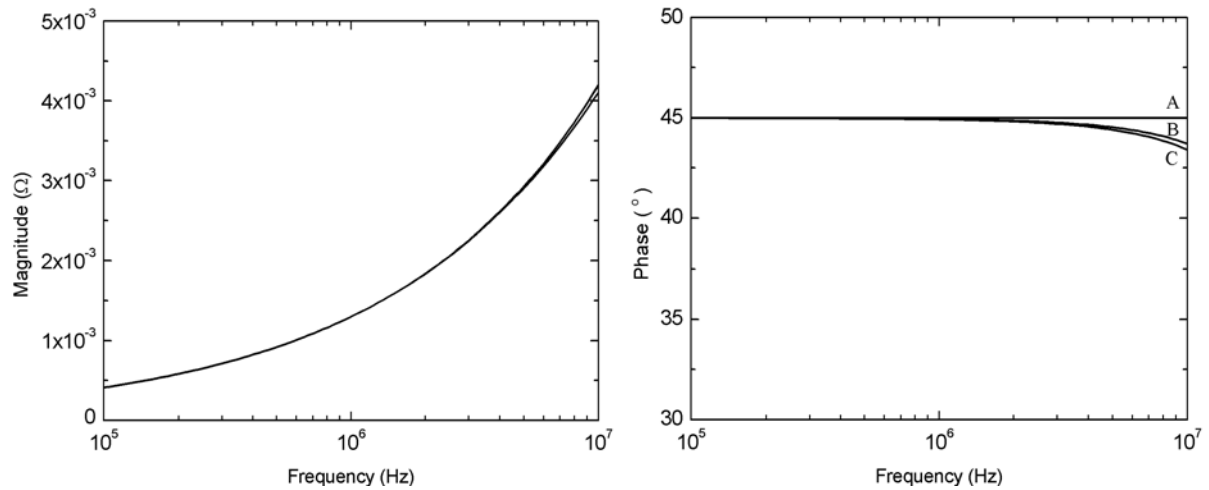
Fig. A2.2. Magnitude and phase of the impedance of the three models of Fig. A2.1, material Suralac 3000: (A) model without insulation, (B) simple insulation model, (C) ladder circuit model.
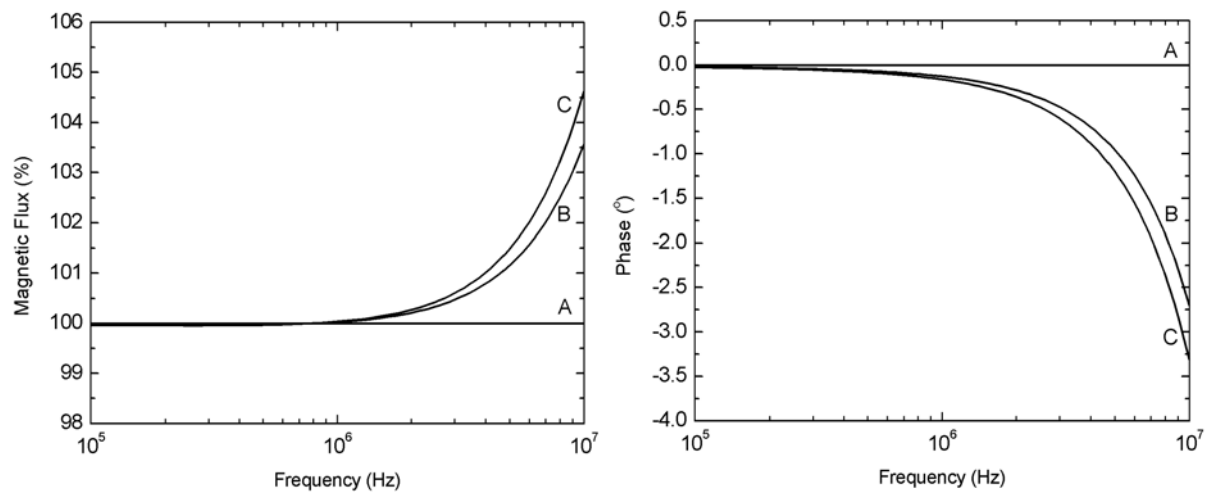

Fig. A2.3. Relative magnitude and phase of the magnetic flux of the three models of Fig. A2.1, material Suralac 3000: (A) model without insulation, (B) simple insulation model, (C) ladder circuit model.
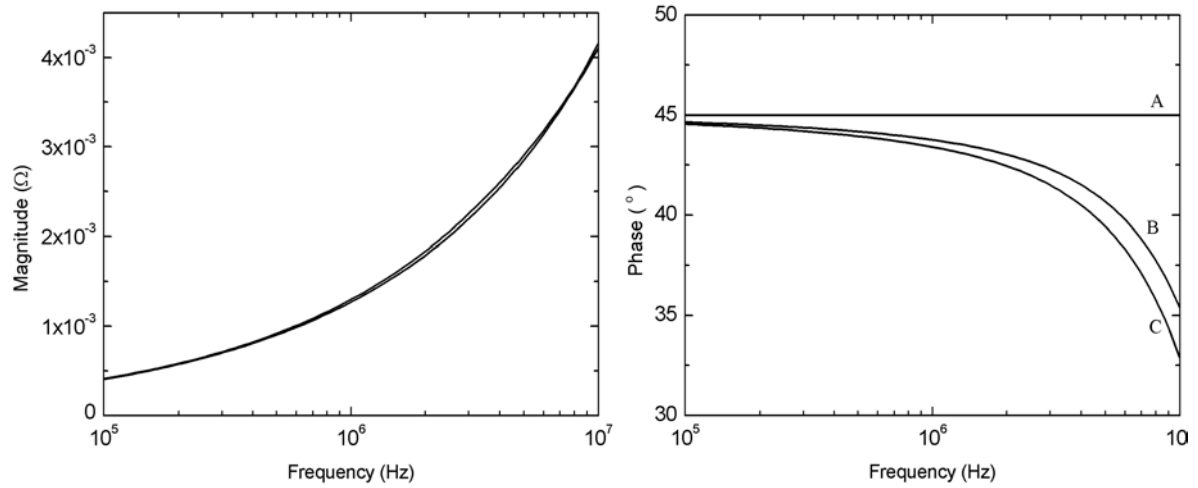
Fig. A2.4. Magnitude and phase of the impedance of the three models of Fig. A2.1, material Suralac 5000: (A) model without insulation, (B) simple insulation model, (C) ladder circuit model.
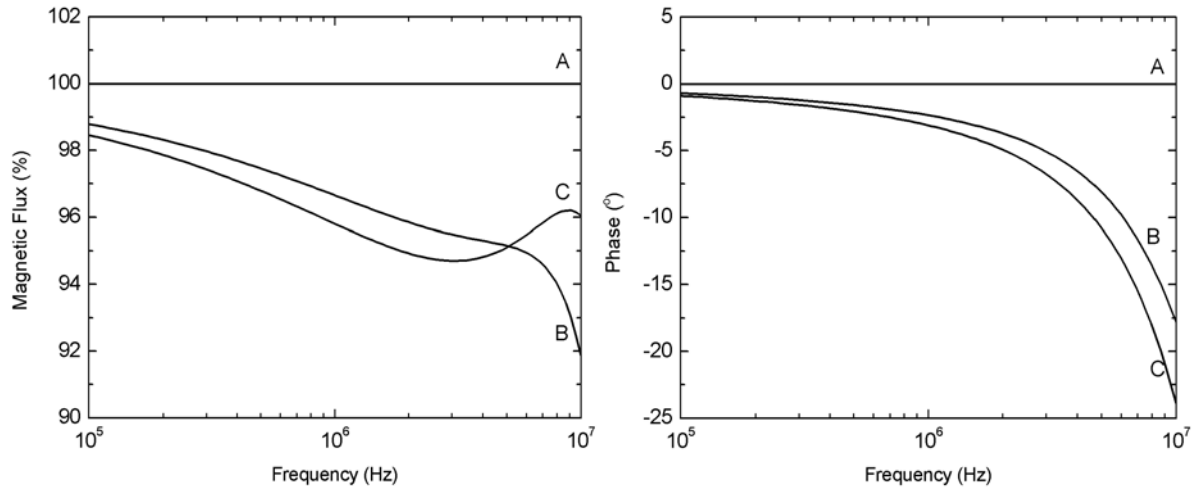

Fig. A2.5. Relative magnitude and phase of the magnetic flux of the three models of Fig. A2.1, material Suralac 5000: (A) model without insulation, (B) simple insulation model, (C) ladder circuit model.